Award Number: W81XWH-08-1-0765

TITLE: Consortium for Bone and Tissue Repair and Regeneration

PRINCIPAL INVESTIGATOR: J. David Eick, Ph.D.

CONTRACTING ORGANIZATION: University of Missouri
Kansas City MO 64108

REPORT DATE: January 2011

TYPE OF REPORT: Final

PREPARED FOR: U.S. Army Medical Research and Materiel Command
Fort Detrick, Maryland 21702-5012

REPORT DOCUMENTATION PAGE

Form Approved
OMB No. 0704-0188

1. REPORT DATE *(DD-MM-YYYY)*	2. REPORT TYPE	3. DATES COVERED *(From - To)*
31-JAN-2011	Final	26 Sep 2008 - 31 Dec 2010

4. TITLE AND SUBTITLE

*Consortium for bone and tissue repair and regeneration

5a. CONTRACT NUMBER

5b. GRANT NUMBER
W81XWH-08-1-0765

5c. PROGRAM ELEMENT NUMBER

6. AUTHOR(S)

J. David Eick, Ph.D.
Email: eickj@umkc.edu

5d. PROJECT NUMBER

5e. TASK NUMBER

5f. WORK UNIT NUMBER

7. PERFORMING ORGANIZATION NAME(S) AND ADDRESS(ES)

University of Missouri
5100 Rockhill Road
Kansas City MO 64108

8. PERFORMING ORGANIZATION REPORT NUMBER

9. SPONSORING / MONITORING AGENCY NAME(S) AND ADDRESS(ES)

U.S. Army Medical Research and Materiel Command
Ft. Detrick, MD 21701

10. SPONSOR/MONITOR'S ACRONYM(S)

11. SPONSOR/MONITOR'S REPORT NUMBER(S)

12. DISTRIBUTION / AVAILABILITY STATEMENT

Distribution is unlimited.

13. SUPPLEMENTARY NOTES

14. Abstract - see next page

14. ABSTRACT

Building upon the considerable strengths of the University of Missouri-Kansas City (UMKC) in biomaterials, biological systems, and clinical expertise and Missouri University of Science and Technology (Missouri S&T) in biomaterials, materials science and engineering, and the engineering disciplines, the Consortium provides a seamless mechanism for designing and developing new biomaterials far exceeding the capacity of the individual groups at each campus. The development of new biomaterials is a joint effort, bringing together life scientists and materials engineers in the development and testing of new biomaterials. The Consortium focuses on the following:

- Speeding up the development of new materials for the repair and regeneration of traumatized bone and tissues by establishing an efficient, shared infrastructure for biomaterials, biosensors, and bio-interfacial research.
- Promoting interdisciplinary collaboration that enhances the rate of scientific discovery and technological advances to develop the next generation of biomaterials and biosensors.
- Developing joint programs to train the next generation of biomedical and biomaterials engineers, providing a future workforce for the US Army and the vital US biotechnology industry.
- Promoting technology transfer and entrepreneurship to commercialize new knowledge, which will improve patient outcomes while expanding economic development in Missouri and the nation.

The proposed project is a collaborative research effort by faculty at UMKC and Missouri S&T for the purpose of creating three-dimensional (3-D) scaffolds composed of bioactive glass fibers, micro-spheres, and particles whose unique structure and properties are optimized for the repair and regeneration of diseased or damaged bones in humans. In addition to being designed to be bioactive and reacting in a biologically beneficial manner with tissue fluids, these 3-D scaffolds will also (1) provide surface features such as high surface area nanostructured hydroxyapatite (HA) that promote cell attachment and proliferation, (2) contain nano- and micro-sized pores conducive to cell growth and function, and (3) release trace elements and protein growth factors that are known to be biologically important to the development of healthy bone. The design, fabrication, and property evaluation of these unique 3-D scaffolds is the primary responsibility of the Missouri S&T faculty participants, with the UMKC faculty providing significant input in the desired biological performance.

The UMKC faculty bears primary responsibility for evaluating and validating the biological performance of the scaffolds in vitro and in vivo and determining how the viability, attachment, proliferation, and differentiation of bone cells is affected by the structural features and chemical properties of a given scaffold. This collaborative work is expected to yield scaffolds that will eventually be evaluated in human experiments, with emphasis on limb and craniofacial applications. Hypothesis: A bioactive 3-D glass scaffold can be developed by the Consortium which will be superior to currently available bone grafting materials and will meet a need of the US Army for advanced biomaterials to repair and regenerate traumatized bone.

KEY RESEARCH ACCOMPLISHMENTS

- Prepared three candidate bioactive glasses with silicate (13-93), borosilicate (13-93B1), and borate (13-93B3) composition, as well as the widely studied silicate 45S5 glass (control);
- Converted three glasses (13-93; 13-93B1; 13-93B3) into porous three-dimensional scaffolds with two different microstructures (described as 'fibrous' and 'trabecular');
- Evaluated the in vitro bioactivity (conversion to a hydroxyapatite-type material in a simulated body fluid) and mechanical response of 13-93, 13-93B1, and 13-93B3 bioactive glass scaffolds with fibrous and trabecular microstructures;
- Evaluated in vitro response of MLO-A5 cells (an established osteogenic cell line) to scaffolds of 13-93 bioactive glass with fibrous and trabecular microstructures;
- Evaluated in vitro response of MLO-A5 cells to bioactive glasses and glass scaffolds of three different compositions (13-93, 13-93B1, and 13-93B3);
- Evaluated the ability of 13-93, 13-93B1, and 13-93B3 bioactive glass scaffolds with the fibrous and trabecular microstructures to support tissue infiltration in a subcutaneous rat implantation model;
- Initiated in vivo experiments: implantation of 13-93 and 13-93B3 scaffolds in dorsal skinfold chambers in rats to assess possible angiogenic responses;
- Initiated in vitro tests of covalently bonding a bioadhesive peptide to 13-93 glass scaffolds as a means of enhancing the attachment, growth, and function of osteogenic cells;
- Prepared scaffolds for implantation into rat calvaria defect model in Year 2, and imaged the scaffolds using microCT on the day of implantation.

15. SUBJECT TERMS

None provided.

16. SECURITY CLASSIFICATION OF:			17. LIMITATION OF ABSTRACT	18. NUMBER OF PAGES	19a. NAME OF RESPONSIBLE PERSON
a. REPORT	b. ABSTRACT	c. THIS PAGE			19b. TELEPHONE NUMBER *(include area code)*
U	U	U	UU	48	

Consortium for Bone and Tissue Repair and Regeneration
Final Report for 09/26/2008–12/31/2010

INTRODUCTION

Building upon the strengths of Missouri University of Science and Technology (Missouri S&T) and the University of Missouri-Kansas City (UMKC), the Consortium was formed to design and develop unique bioactive glass scaffolds which will meet a need of the US Army for advanced biomaterials to repair and regenerate traumatized bone. The **hypothesis** of the research is that three-dimensional bioactive glass scaffolds can be developed by the Consortium which will be superior to currently available bone grafting materials. In addition to being designed to be bioactive and reacting in a biologically beneficial manner with tissue fluids, these scaffolds will also (1) provide surface features such as high surface area nanostructured hydroxyapatite (HA) that promote cell attachment and proliferation, (2) contain nano- and micro-sized pores conducive to cell growth and function, and (3) release trace elements and protein growth factors that are known to be biologically important to the development of healthy bone. This collaborative effort is expected to yield scaffolds that will eventually be evaluated in human experiments, with emphasis on limb and craniofacial applications.

BODY

The research accomplishments associated with the tasks/objectives for the project are described in the following sections.

Objective A: Preparation of Bioactive Glasses (Missouri S&T)

Four glasses, designated 45S5, 13-93, 13-93B1, and 13-93B3, with the compositions given in **Table I** were prepared by conventional glass melting and casting procedures, as described in our previous work (Huang et al., 2006). Glass rods (~10 mm in diameter) were formed by casting the molten glass in steel dies. These rods were sliced with a low-speed diamond saw to produce discs (1 mm thick) to be used in subsequent cell culture studies. Short fibers and particles of the glasses were formed for subsequent preparation of porous scaffolds. The molten glass was first quenched on stainless steel plates. Fibers were prepared by re-melting the glass for 1 h at 1200°C–1400°C, drawing fibers (diameter = 100–300 μm) from the melt, and chopping the fibers to a length of 3 ± 1 mm). Particles (<5–10 μm) were prepared by crushing the quenched glass in a hardened steel mortar and pestle, sieving through stainless steel sieves to give particles <150 μm, and attrition milling for 2 h (**Fig. 1**).

Table I. Nominal composition (in wt%) of bioactive glasses used in this project.

Glass	SiO_2	B_2O_3	Na_2O	K_2O	MgO	CaO	P_2O_5
45S5	45.0	-	24.5	-	-	24.5	6.0
13-93	53.0	-	6.0	12.0	5.0	20	4.0
13-93B1	34.4	20.0	5.8	11.6	4.9	19.5	3.9
13-93B3	0	56.6	5.5	11.1	4.6	18.5	3.7

Objective B: As-prepared Glass Surface vs. Pre-reacted (Incubated) Surface (UMKC)

Discs of 45S5, 13-93, 13-93B1, and 13-93B3 (prepared in Objective A) were sterilized with 70% ethanol for 1 hr, air dried, and then coated with collagen for 1 hr before air drying. The bioactive glass discs were tested with and without pre-incubation in media to determine if pre-reaction in culture media would have an effect on bone cell proliferation. The cells were plated on the discs at 3.5×10^4 cells/well using alpha MEM/5%FBS/5%CS. Cells plated on the plastic surface were used as a positive control. After 24 and 48 hrs, the media was removed and the cells released with trypsin/EDTA and counted using a Coulter Counter. The results are shown in **Fig. 1**. With no pre-incubation (**Fig. 1a**), essentially no toxicity was observed with 45S5 as expected, nor with 13-93 or 13-93B1. However 13-93B3 was toxic, most likely due to the increased percentage of borate. With 4 hrs pre-incubation in culture media, the toxicity of 13-93B3 was reduced, but still evident at 48 hrs (**Fig. 1b**). Experiments were performed to determine the effects of the bioactive glasses on a marker of osteoblast differentiation and function, alkaline phosphatase enzyme activity (**Fig. 2**). The 13-93 and 13-93B1 were similar if not slightly better than the 45S5, but the 13-93B3 had toxic effects on the cells.

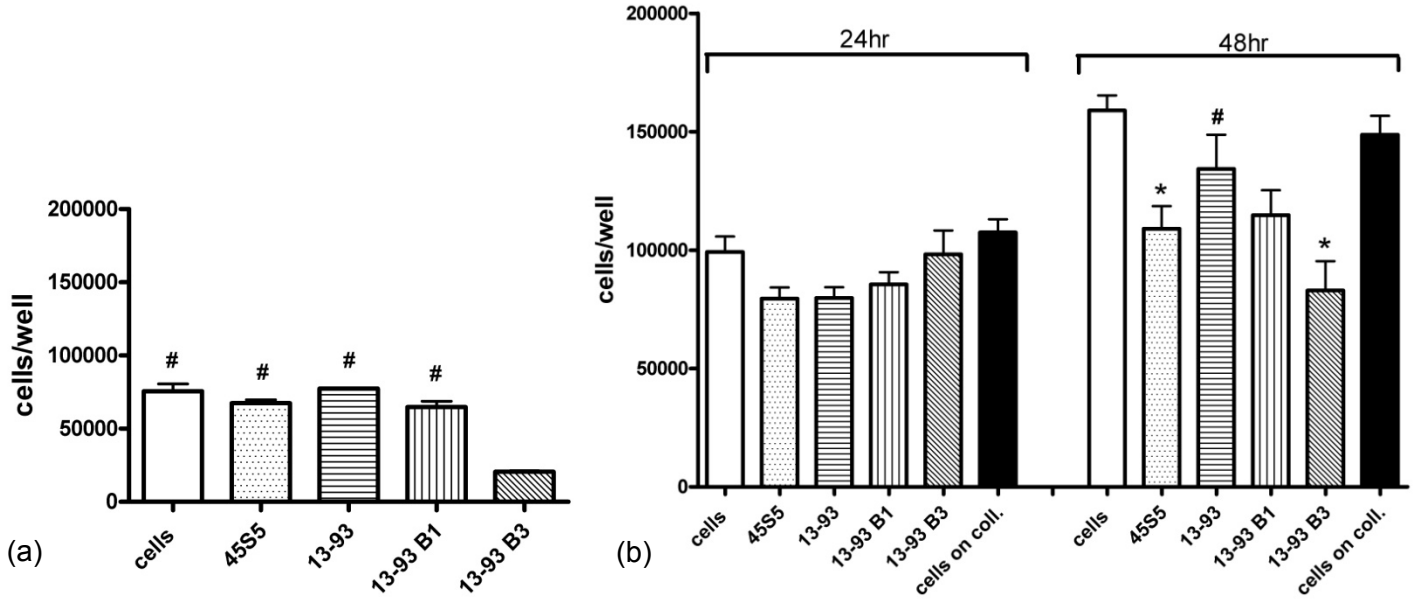

Fig. 1. Effects of silicate 45S5, silicate 13-93, borosilicate 13-93B1, and borate 13-93B3 glass on proliferation of MLO-A5 bone cells. (a) Cells cultured for 24 h on disks without pre-incubation, (n=3) and (b) for 24 and 48 h with pre-incubation for 4 h in media (n=4). Cells plated on plastic control wells (denoted cells) or cells on collagen were used as controls. (n=3) # $p<0.001$ compared to 13-93B3 for (a). *$p<0.05$ compared to cells, # $p<0.05$ compared to 13-93B3 for (b). Significance based on OneWay ANOVA, followed by Tukey post-test. (Bonewald, UMKC).

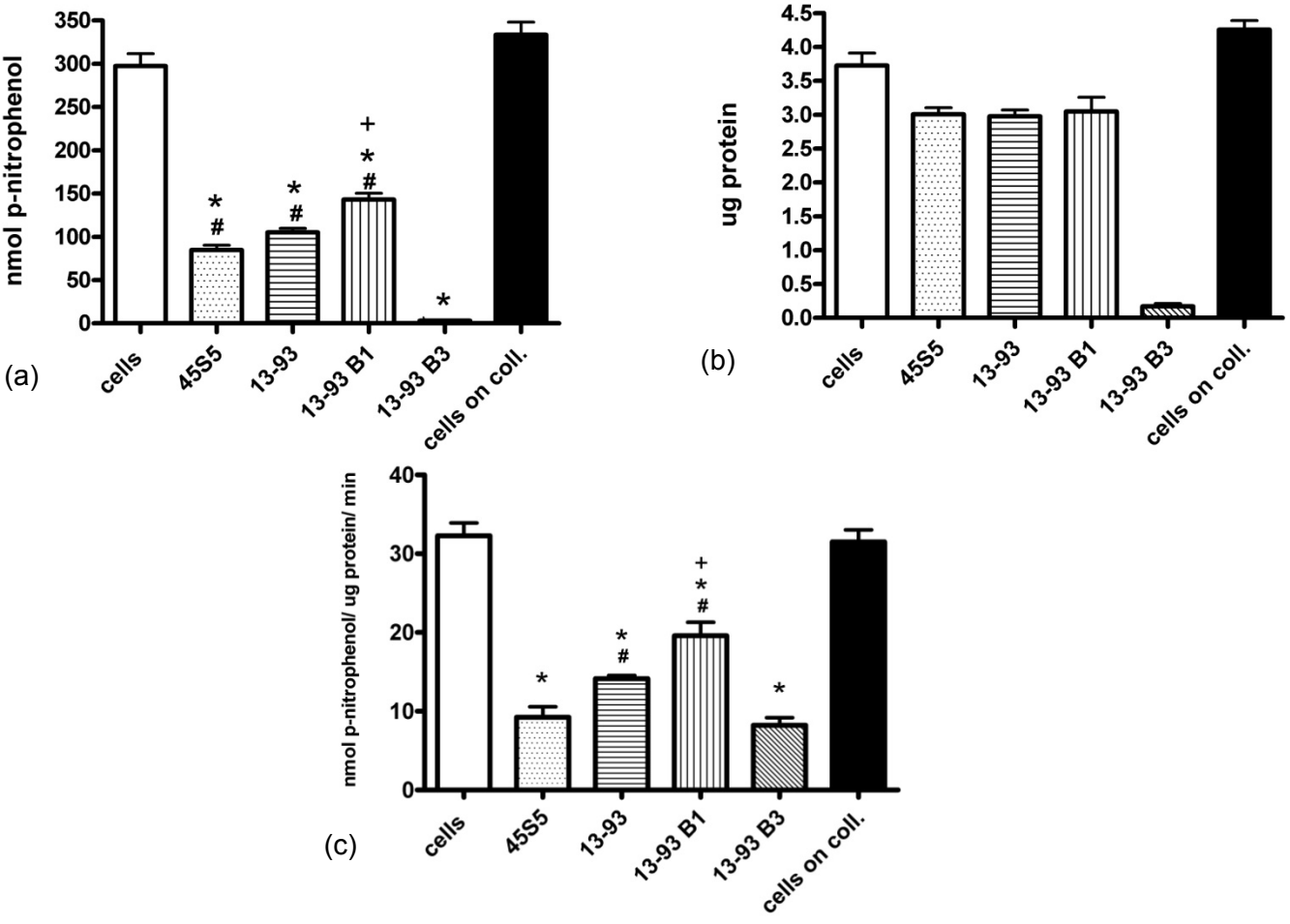

Fig. 2. Effects of 45S5, 13-93, 13-93B1, and 13-93B3 glass on alkaline phosphatase enzyme activity at day 4 of culture of MLO-A5 cells. (a) Enzyme activity in nmole p-nitrophenol activity, $p<0.01$ compared to 45S5, *$p<0.001$ compared to cells, # $p<0.001$ compared to 13-93B3), (b) Protein and (c) enzyme specific activity (+$p<0.001$ compared to 45S5, *$p<0.001$ compared to cells, # $p<0.05$ compared to 13-93B3, $p<0.05$ of 13-93 vs. 13-91B1). Cells plated on plastic control wells (denoted cells) or cells on collagen were used as controls. (n=4). (Bonewald, UMKC).

Objective C: Preparation of Scaffolds (Missouri S&T)
Porous three-dimensional scaffolds of each glass (45S5, 13-93, 13-93B1, and 13-93B3) with two different microstructures, referred to as 'fibrous' and 'trabecular', were prepared at Missouri S&T.

Fibrous scaffolds: Porous scaffolds with a fibrous microstructure were prepared by pouring short fibers randomly into a circular ceramic mold, gently tapping the mold to settle the fibers, and sintering in air for 45 min at 720°C. Scaffolds 7 mm in diameter × 2 mm were prepared for evaluation of the microstructure and biocompatibility, whereas scaffolds 7 mm in diameter × 14 mm were prepared for mechanical testing. **Figure 3** shows SEM images of the 'fibrous' scaffolds with the 13-93 composition. The porosity of the scaffolds (open porosity), as measured by the Archimedes method was 45–50%, while the and a pore size, measured using image analysis of cross sections, was >100 μm. Scaffolds of the 13-93B1, and 13-93B3 bioactive glasses similar microstructures.

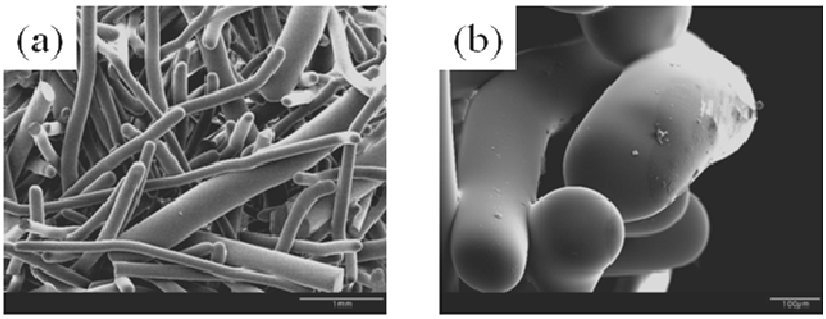

Fig. 3. SEM images of (a) 13-93 bioactive glass scaffold with a 'fibrous' microstructure, and (b) higher magnification image of the scaffold showing the bonds between 13-93 glass fibers. (Day, Missouri S&T)

The compressive strength of the fabricated scaffolds was measured using an Instron testing machine (Model 4204; Instron Corp., Norwood, MA), at a crosshead speed of 0.5 mm/min The scaffolds were tested in accordance with ASTM standard D695-02a (Standard Test Method for Compressive Properties of Rigid Plastics), which was cited as an approved method in ASTM standard F-2150-02 Standard Guide for Characterization and Testing of Biomaterial Scaffolds Used in Tissue-Engineering Medical Products. Ten scaffolds were tested for each group. **Figure 4** shows the stress vs. deformation response for the 'fibrous' 13-93 bioactive glass scaffold. The compressive strength, taken as the highest stress in the curve was ~ 5 MPa.

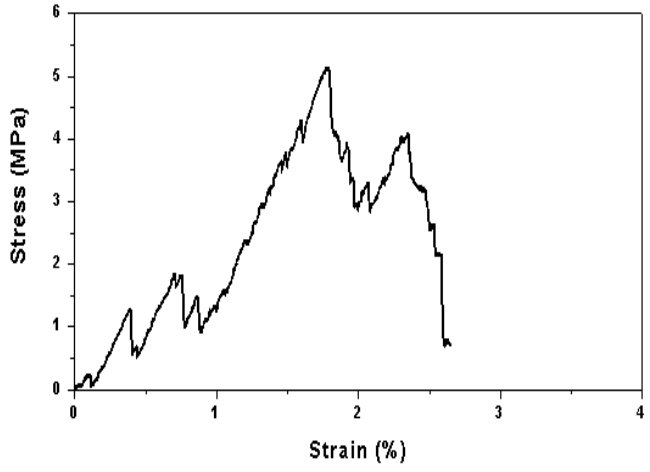

Fig. 4. Stress vs. deformation response in compressive loading for 13–93 bioactive glass scaffolds with a 'fibrous microstructure. (Day, Missouri S&T)

Trabecular scaffolds: Trabecular scaffolds, with a microstructure similar to that of dry human trabecular bone, were prepared using a polymer foam replication technique, as described in detail elsewhere (Fu et al., 2008). Briefly, a commercial polyurethane foam with the requisite pore structure was infiltrated with a stabilized slurry of glass particles (prepared in Objective A). After drying, the particle-coated foams were subjected to a controlled heat treatment to first decompose the foam and then sinter the glass into a dense network. The heating schedule was 1°C/min to 500°C in O_2 gas, then 5°C/min to the sintering temperature: 1 h at 700°C for 13-93, 630°C for 13-93B1, and 570°C for 13-93B3. Trabecular scaffolds of 45S5 glass prepared using this method crystallized during sintering, which limited the sintering of the glass particles, resulting in scaffolds with low strength. **Figure 5** shows scanning electron microscope (SEM) images of the 13-93, 13-93B1, and 13-93B3 scaffolds with the trabecular microstructure. The scaffolds had open porosity of 75–85%, as determined using the Archimedes method, and pores sizes in the range 100–500 μm, as determined using mercury porosimetry. These pore characteristics satisfy the requirements (open porosity >50–60%; mean pore size >100–150 μm) which are considered to be favorable to permit tissue ingrowth and function in porous scaffolds.

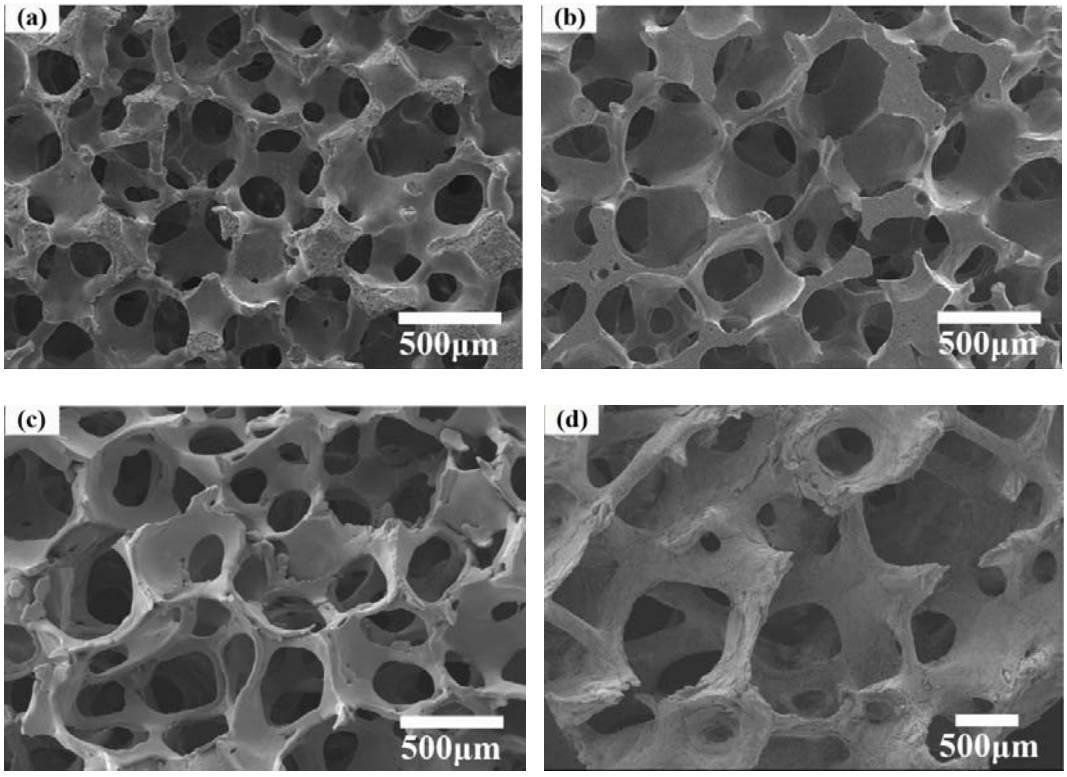

Fig. 5. SEM images of (a) 13-93, (b) 13-93B1, and (c) 13-93B3 bioactive glass scaffolds prepared by the polymer foam replication method. (d) SEM image of a dry human trabecular bone is shown for comparison. (Rahaman, Missouri S&T).

Bioactivity of scaffolds: The bioactivity of the trabecular scaffolds was evaluated by measuring their rate of conversion to a hydroxyapatite-type material in a simulated body fluid (SBF) at 37°C. The composition of the SBF was identical to that described by Kokubo et al. (1990). The conversion reaction is accompanied by a weight loss of the scaffolds, as well as a change in pH value of the SBF, so the kinetics of conversion were determined by measuring these two quantities as a function of time. For both the fibrous and trabecular scaffolds, the glass composition had a marked effect on their *in vitro* bioactivity (**Fig. 6**). The weight loss of the scaffolds increased with increasing B_2O_3 content of the glass (**Fig. 6a**). Concurrently, the pH of the SBF also increased markedly with the B_2O_3 content of the scaffold (Fig. **6b**).

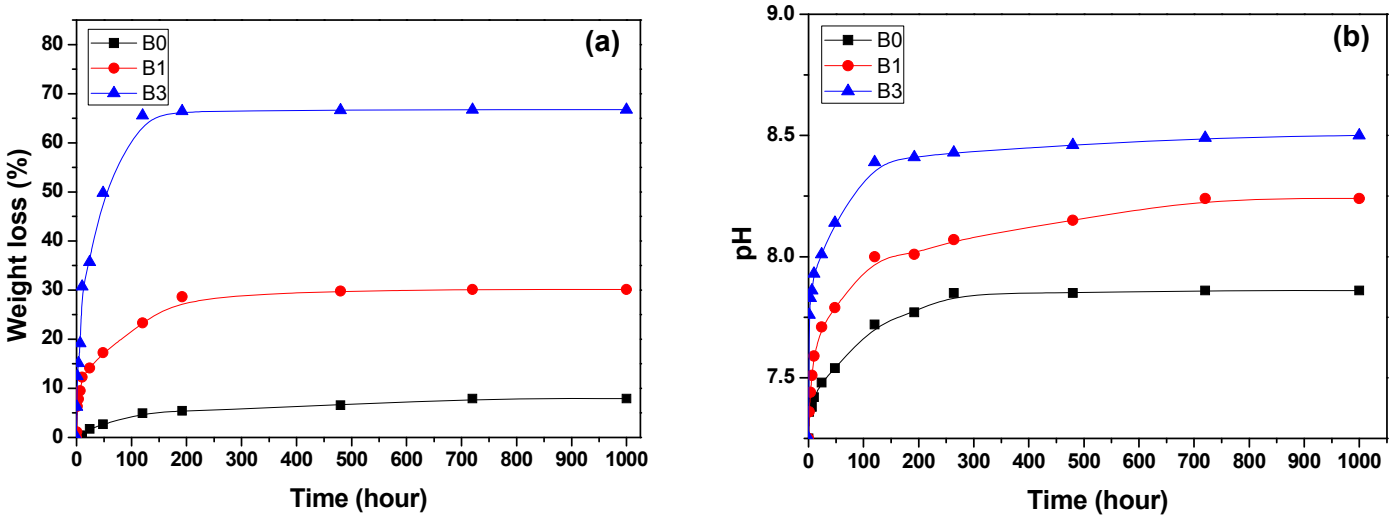

Fig. 6. (a) Weight loss of the scaffold and (b) pH of SBF as a function of immersion time of immersion time of 13-93(B0); 13-93B1, and 13-93B3 scaffolds in a simulated body fluid (SBF). (Rahaman, Missouri S&T).

Figure 7 shows the converted layer on the scaffold surface after 14 days in the SBF. The layer consisted of a porous network of nanometer-sized particles, in which the morphology of the particles changed from needle-like for the 13-93 scaffold to a more spherical shape for the 13-93B3 scaffold. X-ray diffraction (XRD) and Fourier transform infrared (FTIR) analysis confirmed that the converted layer was HA.

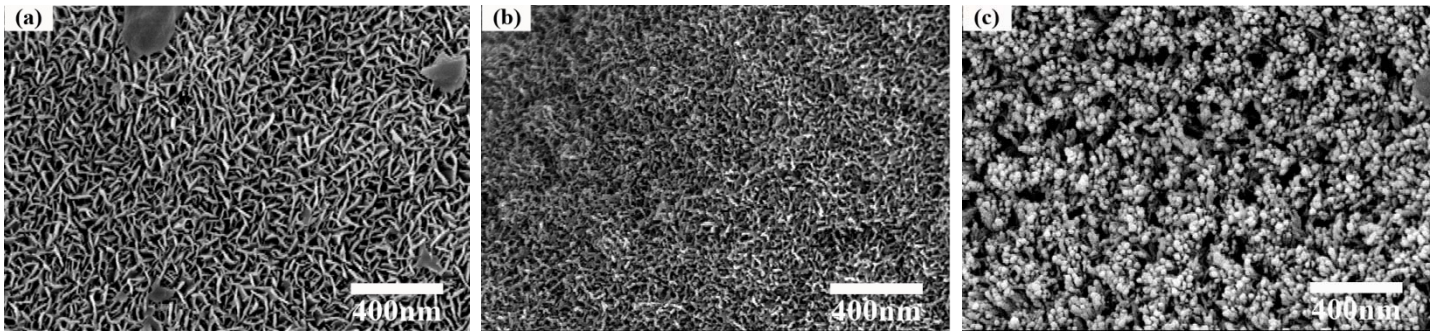

Fig. 7. SEM images of the surface of (a) 13-93 (B0), (b) 13-93B1 and (c) 13-93B3 glass scaffolds after immersion in SBF for 14 days (Rahaman, Missouri S&T).

Mechanical response of scaffolds: Trabecular scaffolds of 13-93, 13-93B1, and 13-93B3 bioactive glass, with a cylindrical shape (6 mm in diameter × 12 mm) were tested in compression (0.5 mm/min) according to ASTM C-773. The scaffolds had a porosity of 75–85% and pores of size 100–500 μm. **Figure 8** shows the stress vs. deformation curves for the 13-93, 13-93B1, and 13-93B3 scaffolds with the trabecular microstructure. The compressive strength, taken as the highest stress on the stress vs. displacement curve, was 11 ± 1 MPa for 13-93, 7.0 ± 0.5 MPa for 13-93B1, and 5.0 ± 0.5 MPa for 13-93B3, showing that the strength decreased with increasing B_2O_3 content of the glass.

When immersed in a SBF, the scaffolds showed a marked decrease in strength as a function of immersion time (**Fig. 9**). The degradation of the strength was dependent on the glass composition. Because of the rapid conversion of the borate 13-93B3 glass to HA, the strength of these scaffolds decreased to almost zero within 4 days. Within the same time, the strength of the as-prepared silicate 13-93 scaffolds decreased to ~30% of its as-prepared strength.

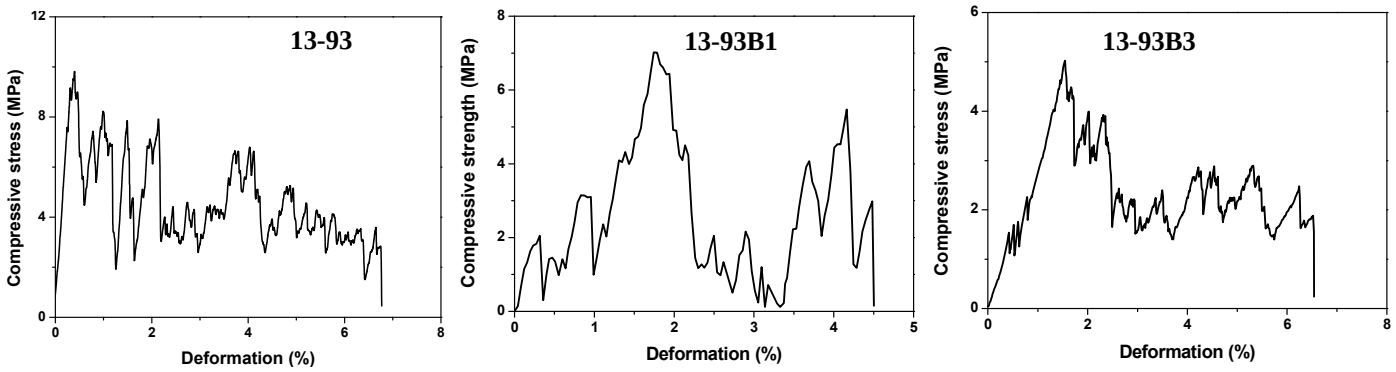

Fig. 8. Stress vs. deformation curves for 13-93, 13-93B1, and 13-93B3 scaffolds with the trabecular microstructure, in compression testing at a deformation rate 0.5 mm/min. (Rahaman, Missouri S&T)

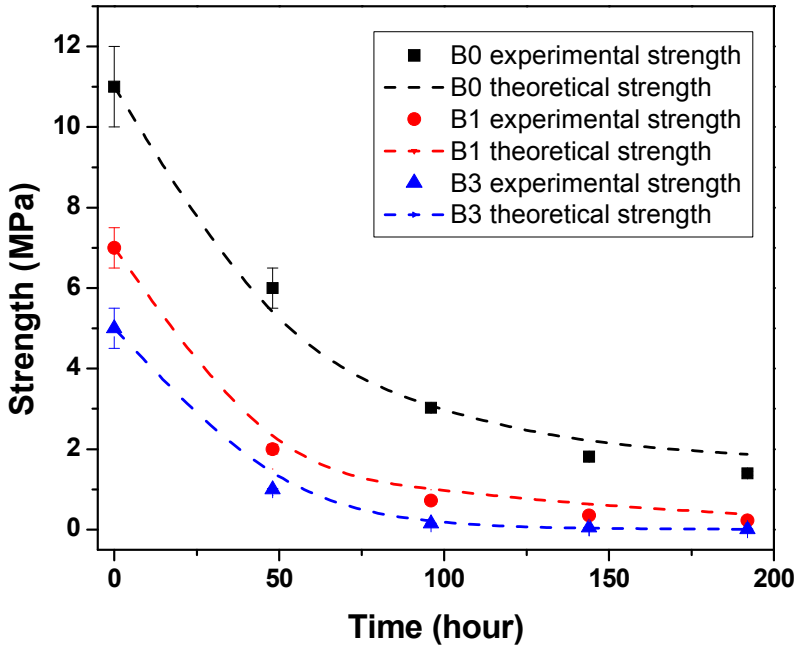

Fig. 9. Compressive strength vs. immersion time in a SBF for silicate 13-93, borosilicate 13-93B1, and borate 13-93B3 scaffolds with the trabecular microstructure (experimental strength). The theoretical strengths were based on a model that compensated for the reduction of the cross-sectional area of the glass struts in the scaffolds resulting from conversion of the glass to a porous HA-type material. (Rahaman, Missouri S&T).

Objective D: Functionalized vs. Non-functionalized Surface (Missouri S&T)

A major item pursued during the second year involved adding the bioadhesive peptide Arg-Gly-Asp-Cys (RGDC) to 13-93 glass scaffolds in an attempt to enhance the attachment, growth, and function of osteogenic cells. Initial tests of the RGDC coating were performed with single ply mats of parallel-oriented of 13-93 glass fibers (Brown et al., 2008). The rationale for use of these simple two-dimensional constructs was to permit use of a standard epi-fluorescence microscope to view attachment of fluorochrome-labeled cells to RGDC coated fibers. The method of adding RGDC involved derivitization of the glass with an aminosilane plus a heterobifunctional cross-linking agent followed by covalent coupling of the RGDC peptide to the derivatized glass by a procedure described elsewhere (Davis et al., 2002). The aminosilane used was 3-aminopropyl-trimethoxysilane and the cross-linking agent is γ-maleimidobutyryloxy-succinimide (GMBS). The 13-93 glass fibers were treated overnight with a 2% solution of aminosilane in 95% EtOH, washed with EtOH, and cured for 1 h at 90 C. The treated glass was incubated for 1 h in 1 mg/ml GMBS to permit the succinimide group of the GMBS to bond to the free amine of the aminosilane. The treated glass fibers were then placed in 0.5 mg/ml RGDC for 1 h to permit covalent attachment of RGDC to the maleimide end of the GMBS cross-linker.

Immediately after washing to remove unbound peptide, the RGDC-coated and companion control 13-93 glass fibers were seeded with 50,000 MLO-A5 osteoblastic cells. After culture intervals of 1 and 3 days, the samples were washed, fixed in cold 100% EtOH, and stained with the DNA-binding fluorochrome Hoechst 33258. The stained samples were then examined on the epifluorescence microscope with a DAPI filter in place to visualize the density and distribution of Hoechst 33258-labeled nuclei. As shown in **Fig. 10**, there was very little increase in cell density density between day 1 and day 3 with the untreated glass fiber mats and mats treated with the aminosilane only. In contrast, there was a dramatic increase in cell density between day 1 and day 3 on the RGDC coated mats. These results confirm the effectiveness of RGDC coating for enhanced growth of osteogenic cells on the 13-93 glass fiber constructs.

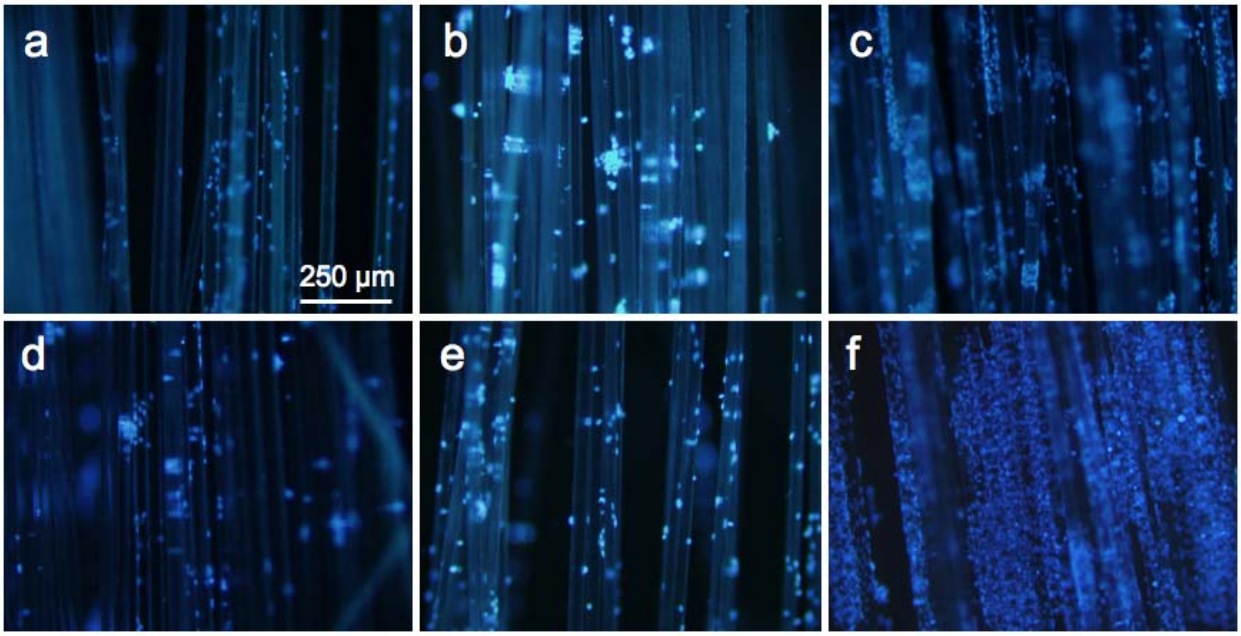

Fig. 10. Fluorescent imaging of relative density of MLO-A5 cells seeded on 13-93 glass fiber rafts after incubations of: (a-c) 1 day; and (d-f) 3 days. The 13-93 rafts were: (a,d) untreated controls; (b,e) aminosilane treated; and (c,f) RGDC coated. The samples were stained with Hoechst 33258 to detect the cells with a DAPI filter used for imaging.

Coating of three dimensional scaffolds with RGDC bioadhesive peptide

Three-dimensional fiber scaffolds were then coated with the RGDC peptide by the same aminosilane/GMBS derivatization procedure used with the two-dimensional glass fiber mats. Two sets of experiments were performed to compare the distribution and relative density of MLO-A5 osteoblastic cells cultured on untreated control and RGDC-coated 13-93 glass fiber scaffolds. The RGDC coated and untreated control scaffolds were each seeded with 35,000 MLO-A5 osteoblastic cells and cultured for intervals of 1, 3, and 5 days with four replicate samples per day. Two of the four replicates were labeled with MTT for the last four hours of incubation. The other two replicates were fixed in cold 100% EtOH, stained for 10 min with the fluorochrome Hoechst 33258 (2 µg/ml), and then examined under a DAPI filter to visualize the density and distribution of Hoechst 33258-labeled nuclei. The two fluorescent images in **Fig. 11** show a comparison of the relative density of fluorochrome-labeled cells within the interior of the scaffolds after three days of incubation. These two images, which are representative of the multiple samples examined, show a noticeably higher density of cells within the RGDC-coated scaffolds compared to the untreated control scaffolds. Although not included here, the pattern of MTT labeling appeared more uniform and more intense for the cell-seeded 13-93 glass fiber scaffolds coated with RGDC compared to the untreated scaffolds.

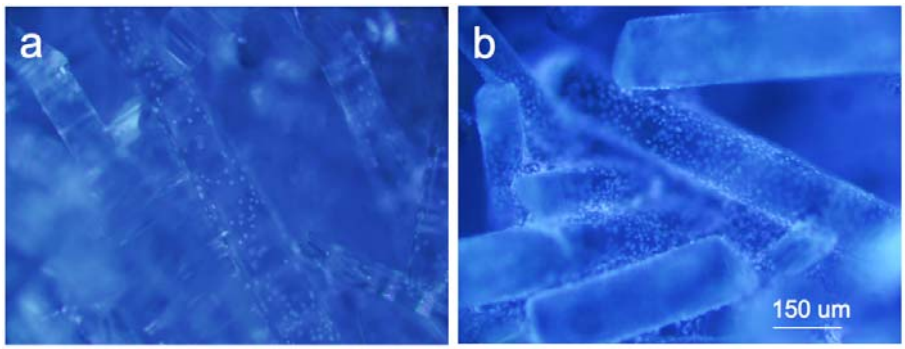

Fig. 11. Fluorescent images of relative densities of MLO-A5 cells incubated for three days on untreated control (a) and RGDC-coated (b) 13-93 glass fiber scaffolds. Imaging with a DAPI filter was used to detect Hoechst 33258-labeled nuclei.

Two additional sets of experiments were performed to compare growth and function of MLO-A5 cells cultured on untreated control and RGDC coated 13-93 glass fiber scaffolds. The scaffolds were seeded with 35,000 MLO-A5 osteoblastic cells and cultured for intervals of 1, 3, and 5 days with three replicate samples per day. Growth was assessed by measurement of total protein and alkaline phosphatase activity was assayed as an indicator of differentiated function. As shown in **Fig. 12** total protein increased approximately linearly during the five day incubation. The amount of total protein was about 1.4-fold higher on the RGDC-coated scaffolds compared to the untreated control scaffolds, a finding that is consistent with the higher cell densities seen in the fluorescent images of the peptide coated scaffolds.

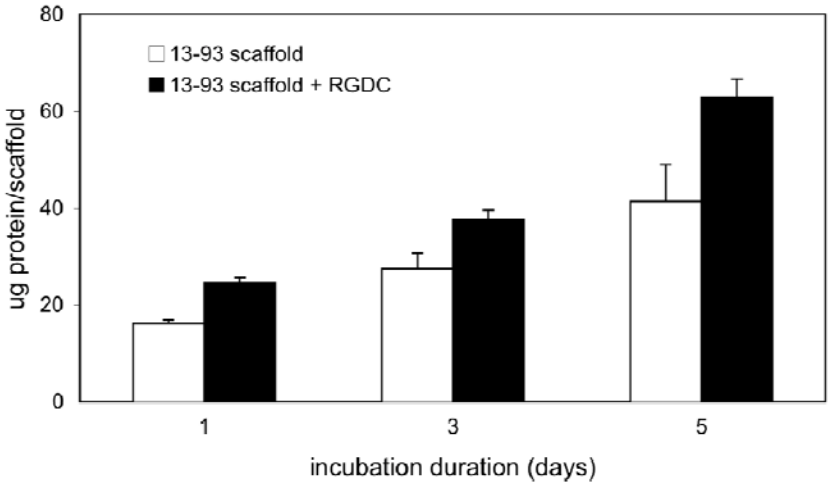

Fig. 12. Growth of MLO-A5 cells cultured on untreated and RGDC coated 13-93 glass fiber scaffolds as determined by measurement of total protein. Each bar represents an average of three replicates ± SD

Results of spectrophotometric measurements of alkaline phosphatase activity in MLO-A5 cells cultured on untreated and RGDC coated 13-93 glass fiber scaffolds for 1, 3, and 5 days are presented in **Fig. 13**. As shown, alkaline phosphatase activity increased during the five day incubation and at a rate greater than the increase in total protein. It is noteworthy that the levels of alkaline phosphatase activity on the peptide-coated 13-93 glass fiber scaffolds is about 2.5 to 3-fold higher compared to the untreated control scaffolds.

The results that have been obtained indicate that coating the 13-93 glass fiber scaffolds with the RGDC bioadhesive peptide does enhance the density and differentiated function of the osteogenic cells seeded onto these constructs. Also, our results at this point seem to indicate the RGDC coating promotes growth within the interior of the porous scaffolds.

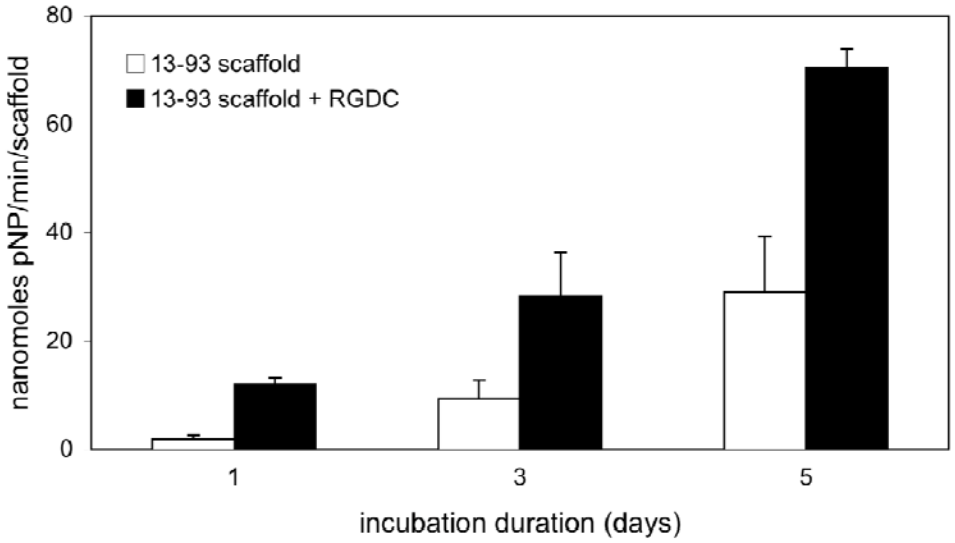

Fig. 13. Total alkaline phosphatase (ALP) activity in MLO-A5 cells cultured on untreated control and RGDC-coated 13-93 glass fiber scaffolds. Enzyme activity is expressed as nmoles of pNP formed per minute per sample and each bar represents the average of three replicates ± SD.

Objective E: In Vitro Cell Culture (Missouri S&T)

The effect of the microstructure and glass composition of the scaffolds on the proliferation and function of MLO-A5 cells, an established osteogenic cell line (Kato et al., 2001), was investigated.

Effect of scaffold microstructure:

Scaffolds of 13-93 glass (~6 mm diameter × ~2.5 mm thick) with the trabecular and fibrous microstructures, prepared as described in Objective C, were dry heat sterilized, preconditioned 1 h in complete medium, blotted dry, and seeded with 50,000 MLO-A5 cells. After cell attachment, the samples were placed in a 24-well plate containing α-MEM medium with 5% fetal bovine serum/5% neonatal calf serum. Incubation was at 37°C in 5% CO_2 with medium changed at 2 day intervals.

SEM visualization: The scanning electron micrographs in **Fig. 14** show the morphology and relative density of MLO-A5 cells on 13-93 fiber and trabecular scaffolds at culture intervals of 2, 4, and 6 days. The cells visible in the images appear well attached on both scaffold types. As a group, the SEM images of **Fig. 14** show a continuing increase in cell density during the 6-day incubation on both the 13-93 fiber and 13-93 trabecular scaffolds, a pattern seen in additional SEM analyses of MLO-A5 cells cultured on these porous constructs.

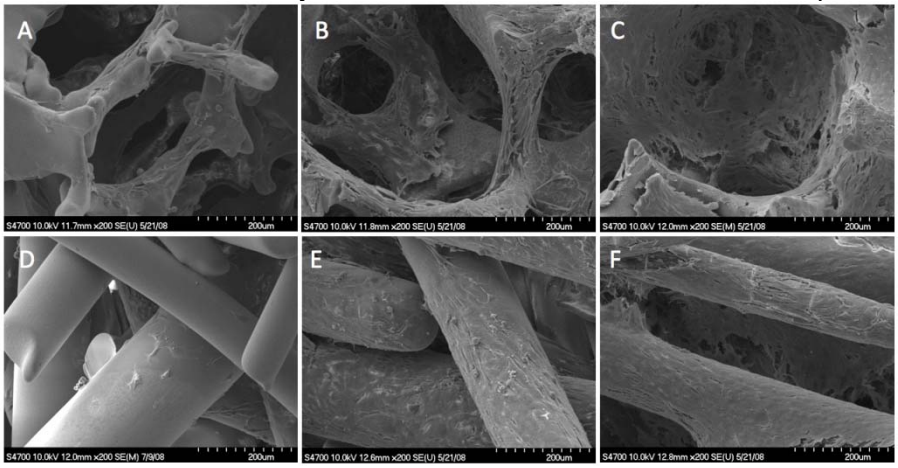

Fig. 14. Scanning electron microscope images of MLO-A5 cells cultured 2 days (A, D), 4 days (B,E), and 6 days (C,F) on fiber scaffolds (A-C) and trabecular scaffolds (D-F). The micrographs show well-attached morphology plus increasing density during the 6 day culture. (Brown, Missouri S&T).

Metabolic activity and growth on scaffolds: The tetrazolium salt MTT was added to cell-seeded scaffolds for the last 4 h of incubations of 2, 4, and 6 days to permit visualization of metabolically active cells on and within the fiber and trabelular scaffolds. The amount of purple formazan, the product of MTT metabolism, visible on the cell-seeded scaffolds increases with incubation duration (**Fig. 15**), an indication of active cell growth on these porous constructs. Particularly noteworthy is the presence of this MTT product within the interior of the scaffolds. The amount of purple formazan visible in the interior, although less than on the surface, suggests there is adequate nutrient permeating the scaffolds to keep cells within the interior in a metabolically active state. The size and interconnectivity of the pores of the fiber and trabecular scaffolds likely accounts for permeation of nutrient and thereby fulfills one of the main properties required for scaffolds designed for use in bone tissue engineering applications.

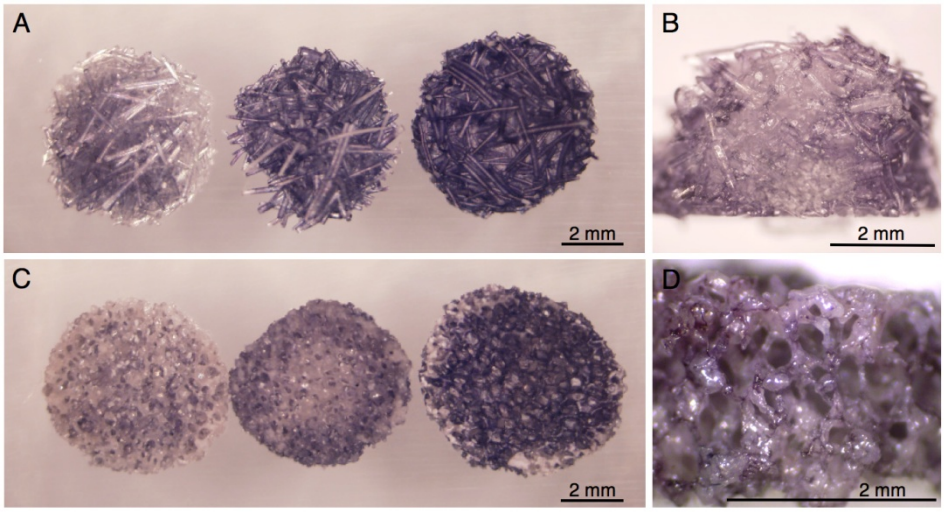

Fig. 15. Bone cell-seeded fiber and trabecular scaffolds treated with MTT for the final 4 h of incubations of 2, 4, and 6 days (panel A and C). The freeze fracture face of cell-seeded fiber and trabecular scaffolds at day 6 are shown in panels B and D, respectively. The latter images show MTT labeled cells within the interior of the scaffolds. (Brown, Missouri S&T).

Total amounts of protein in cellular material recovered from MLO-A5 cells cultured on the fiber and trabecular scaffolds were measured as an additional assessment of ability of the scaffolds to support cell growth. As shown in **Fig. 16**, the amount of protein recovered from the scaffolds increased at a nearly linear rate, a finding that complements the increase in cell density observed in the SEM images.

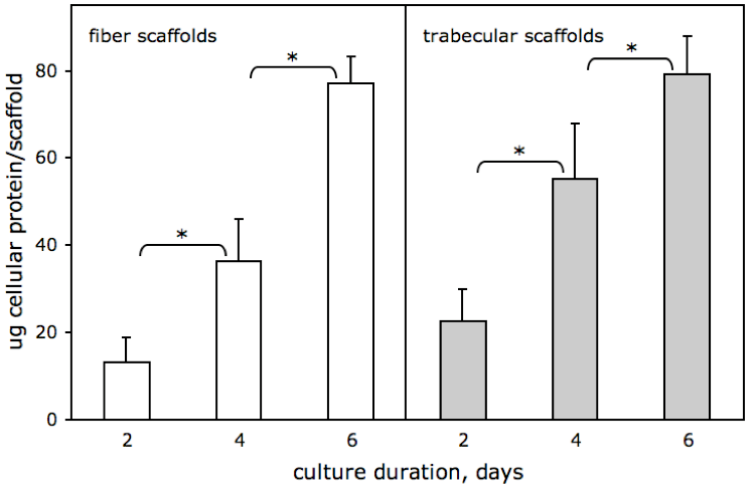

Fig 16. Cell proliferation on 13-93 fiber and trabecular scaffolds assessed by quantitative measurement of total protein. Each bar represents an average of three replicates ± SD. The asterisks indicate statistically significant differences in total protein between culture intervals (p<0.05).

Alkaline phosphatase activity in scaffold cultures: A requirement of scaffolds used for bone tissue engineering applications is the ability to support differentiation of osteoprogenitor cells to functional bone tissue. Alkaline phosphatase (ALP) activity, a well-characterized indicator of the osteogenic phenotype, was measured in MLO-A5 cells cultured on the 13-93 fiber and trabecular scaffolds as a test of differentiated function. Results of spectrophotometric measurements of ALP activity in cell lysates recovered from the scaffolds at culture intervals of 2, 4, and 6 days are presented in **Fig. 17**. As shown, ALP activity increased extensively in these cells with the duration of incubation on the scaffolds. This finding is an indication that the fiber and trabecular scaffolds do effectively support one activity associated with osteogenic function.

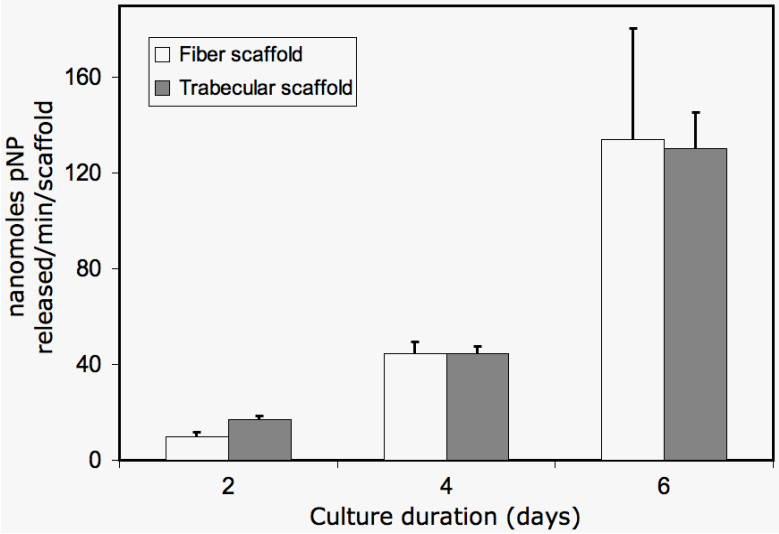

Fig. 17. Alkaline phosphatase activity in MLO-A5 cells cultured on 13-93 glass fiber and trabecular scaffolds. Enzyme activity is expressed as nmol of pNP per minute per scaffold. Average of 3 replicates ± (SD). (Brown, Missouri S&T).

Mineralization on scaffolds: Formation of a mineralized matrix is a defining indicator of the osteogenic phenotype and one of the properties of MLO-A5 cells incubated for an extended duration in mineralization medium (supplemented with ascorbic acid and ß-glycerolphosphate). Measurements of alizarin red staining of mineralized nodules formed by MLO-A5 cells cultured on fiber and trabecular scaffolds are presented in **Fig. 18**. As shown, the addition of mineralization inducing medium caused formation of alizarin red-positive material to increase almost twenty fold compared with that in scaffold cultures maintained in normal control medium. This is further evidence that the 13-93 fiber and trabecular scaffolds support osteogenic differentiation.

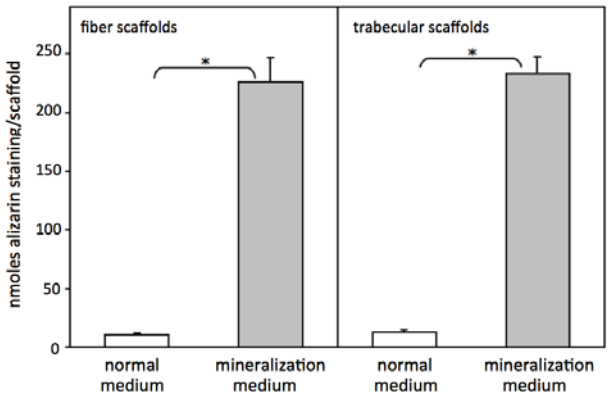

Fig. 18. Comparison of alizarin red staining of mineralized matrix formed by MLO-A5 cells cultured for 12 days on 13-93 fiber and trabecular scaffolds in normal medium vs. mineralization inducing medium. n=3. (Brown, Missouri S&T).

MTT cytotoxicity assay of glass extracts

The 13-93; 19-93B1; and 13-93B3 glasses were pulverized to ≤45 um particles, dry heat sterilized, and then incubated for two days at 50˚C in nanopure water at a concentration of 30 mg/ml. The pH of the resulting aqueous extracts of the 13-93; 19-93B1; and 13-93B3 glasses were found to be 7.8, 9.0, and 9.1, respectively. A portion of each glass extract was adjusted to pH 7.4 and then filter sterilized. Appropriate volumes of the original extract and pH adjusted extract of each glass were added to complete α-MEM medium containing 10% fetal bovine serum. The quantitative cytotoxic assay involving mitochondrial reduction of MTT tetrazolium was used to assess effect of the extracts. MLO-A5 cells were seeded at 5200 cells/well in α-MEM medium with various amounts of the extract in 96-well plates. After 3 days of incubation, MTT was added (50 µg/well) for the last 4 h of incubation. Amounts of purple formazan product formed was measured at 550 nm in a plate reader.

Effects of the addition of original extract and pH adjusted extract of the 13-93, 13-93 B1, and 13-93 B3 glasses are shown in the **Figs. 19 and 20**, respectively. The level of proliferation of MLO-A5 cells cultured in medium containing the original extract and the pH adjusted extract of the standard 13-93 glass was 94 to 105% of control over a wide range of test concentrations (from 0.2 to 10 mg/ml). Addition of increasing amounts of original extract of the 13-93 B1 glass caused a concentration-dependent partial inhibition of MLO-A5 cell growth dropping to approximately 60% of control at glass concentrations of 10 mg/ml. Increasing amounts of neutralized extract of the 13-93 B1 glass caused similar levels of partial inhibition of growth dropping to approximately 65% of control at 10 mg/ml. Incubation of MLO-A5 cell in the presence of the 13-93 B3 glass extracts caused a more dramatic concentration-dependent inhibition of growth. Addition of the original extract and the pH adjusted extract of 13-93 B3 glass at 10 mg/ml decreased cell growth to 18% and 23% of control, respectively.

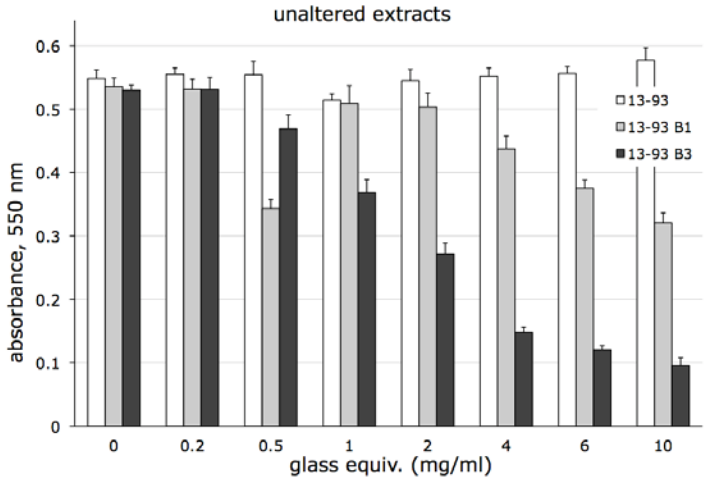

Fig. 19. Evaluation of cytotoxicity of unaltered extracts of 13-93, 13-93B1, and 13-93B3 glasses by MTT hydrolysis. Each bar represents MTT formazan product formed MLO-A5 cells cultured with extract and is an average of five replicates ± SD. (Brown, Missouri S&T).

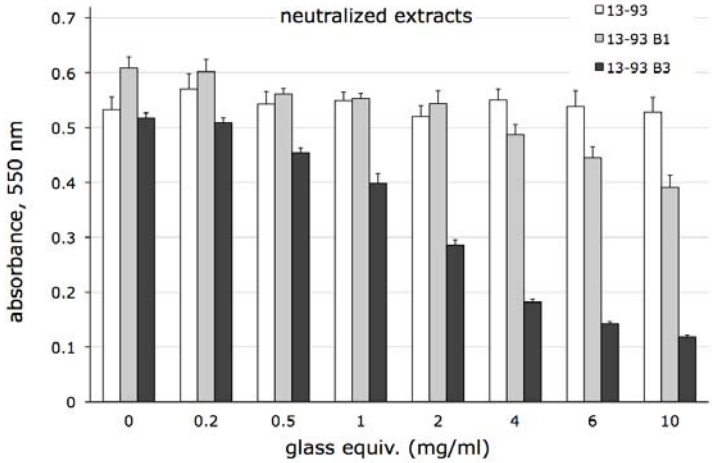

Fig. 20. Evaluation of cytotoxicity of neutralized extracts of 13-93, 13-93B1, and 13-93B3 glasses by MTT hydrolysis. Each bar represents MTT formazan product formed MLO-A5 cells cultured with extract and is an average of five replicates ± SD. (Brown, Missouri S&T).

It was apparent from these tests that the 13-93 B1 glass cause a modest inhibition of cell proliferation, the 13-93 B3 glass causes a more severe inhibition of cell proliferation, and the extract of the standard 13-93 glass has no discernable effect. It was noteworthy that for each of these glass compositions, the levels of inhibition of cell growth by the original unaltered extracts and the neutralized extracts were nearly the same. These and other related results suggest that the modest to severe inhibition of cell growth by 13-93 B1 and 13-93 B3 glasses occurs by a mode of action other that a pH effect.

Assessment of biocompatibility

An additional procedure used to compare the relative levels of biocompatibility of the 13-93, 13-93 B1, and 13-93 B3 glasses was a qualitative assay of cell morphology and density. MLO-A5 cells were seeded in 12-well plates in α-MEM medium with 6 mg/ml of the various extracts. After incubations of 1 day and 3 days, the cell morphologies and relative densities of the cells were compared to qualitatively assess the biocompatibility of the glass extracts.

Representative images of the morphology and relative densities of MLO-A5 cells after 1 day and 3 days of culture in the presence of 13-93, 13-93 B1, and 13-93 B3 extracts are shown in **Fig. 21**. Cells incubated with 13-93 extract are well attached to the plate, show the spread, attached morphology characteristic of the MLO-A5 cell line, and underwent dramatically increased cell density between day 1 and day 3. Cells incubated with the 13-93 B1 extract have a lesser increase in cell density and do not show the typical morphology. Incubation with the 13-93 B3 extract resulted in rounded, poorly-attached cells with very little increase in cell density between day 1 and day 3. Overall these results reveal the 13-93 B1 glass has reduced biocompatibility compared to the standard 13-93 glass while the 13-93 B3 compositions is clearly cytotoxic.

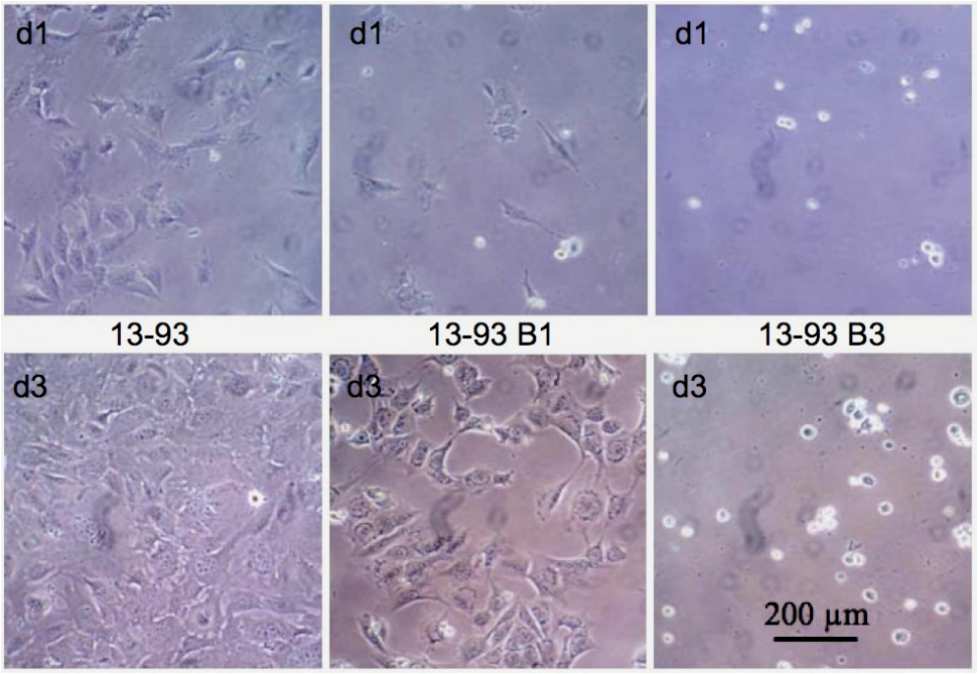

Fig. 21. Phase contrast images of MLO-A5 cells in medium with neutralized extracts of 13-93, 13-93B1, and 13-93B3 glass (6 mg/ml) at d1 and d3 of culture. (Brown, Missouri S&T).

Static vs. dynamic culture of MLO-A5 cells

As part of this phase of the project, tests were performed to compare cell growth on the scaffolds during incubation under two conditions. One was standard incubation with cell-seeded scaffolds in non-mobile 60 mm dishes ('static') in the CO_2 incubator. The second condition was with scaffolds in dishes on a platform rocker

set at 30 oscillations/min and positioned in the CO_2 incubator ('dynamic'). Following a 4-day incubation under the static and dynamic conditions, MLO-A5 seeded scaffolds were labeled with MTT. The static incubation resulted in labeling mostly on the scaffold surface with much less labeling in the interior. In contrast, the dynamic incubation yielded more homogeneous labeling with dark purple formazan product visible nearly uniformly throughout the scaffold suggesting that the dynamic incubation allowed greater delivery of nutrient to cells in the exterior thereby allowing a more uniform growth.

In a similar manner, dynamic incubation was tested as a way of enhancing growth of MLO-A5 cells on 13-93 B3 glass scaffolds, the glass with very low biocompatiblility. The photograph image in **Fig. 22** compares the pattern of MTT labeling of MLO-A5 seeded 13-93 B3 scaffolds after 2 day culture under static and dynamic conditions. The static incubation resulted in very little labeled with MTT. In contrast, the dynamic incubation yielded much greater labeling with MTT indicating the presence of more cells on the scaffolds. This indicates the dynamic incubation allowed reduction of the toxicity of the 13-93 B3 glass.

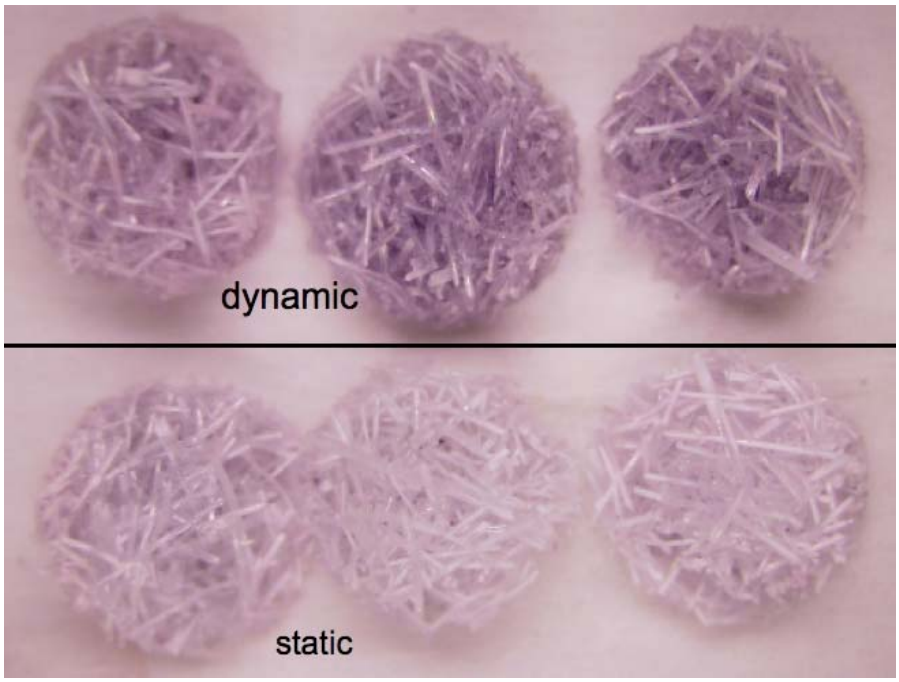

Fig 22. MTT labeling of cell-seeded 13-93 B3 scaffolds incubated 2 days under dynamic and static conditions. (Brown, Missouri S&T).

Effect of scaffold glass composition:
The composition of the glass scaffold also had a marked effect on its ability to support proliferation and function of MLO-A5 cells.

Scaffolds of 13-93, 13-93B1 and 13-93B3 bioactive glass (6mm in diameter × 2 mm thick) with the trabecular microstructure were sterilized by washing 3 times with water and ethanol (for 13-93 and 13-93B1 compositions) or ethanol (for 13-93B3 composition), followed by heating for 24 h at 500ºC. The scaffolds were each seeded with 50,000 MLO-A5 cells suspended in 40 µl medium. After incubating for 4 h to permit cell attachment, the cell-seeded scaffolds were transferred to a 24-well culture plate containing 2 ml of complete medium per well. At selected time intervals, the glass scaffolds with attached cells were removed for assays.

Cell viability: The effect of glass composition on the viability of MLO-A5 cells was assessed using a live cell/dead cell assay. After culturing for different intervals, the trabecular scaffolds with attached cells were rinsed gently with warm phosphate-buffered saline (PBS), and incubated for additional 30 min in 2 ml serum-free medium containing 2 µM calcein AM and 2 µM ethidium homodimer, EthD-1 (Invitrogen Corp, Carlsbad, CA). The fluorochrome labeling of the MLO-A5 cells showed a marked increase in cell number with culture time for the 13-93 and 13-93B1 scaffolds, with very few dead cells (**Fig. 23**). On the other hand, no increase in

cell number was observed for the 13-93B3 scaffolds, and a few dead cells were found on these scaffolds at all culture times. These cell viability results for the porous scaffolds are consistent with the results in Fig. 1a for cell proliferation of MLO-A5 cells on dense discs of 13-93, 13-93B1, and 13-93B3 glass.

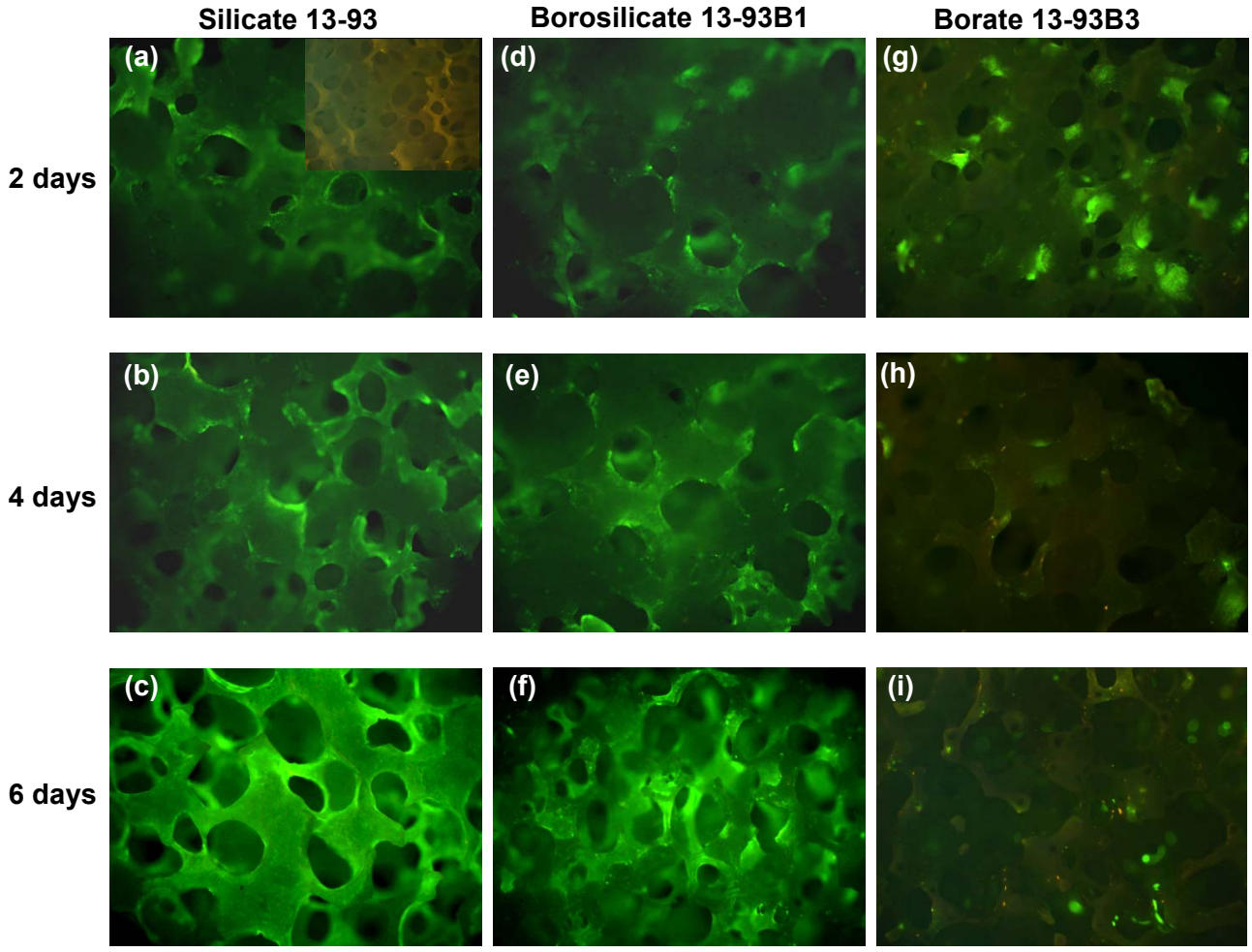

Fig. 23. Fluorescent images of MLO-A5 cells cultured on 13-93, 13-93B1, and 13-93B3 scaffolds (left to right) for 2, 4, and 6 days (top to bottom). The inset in (a) shows an image of a 13-93 scaffold without cells. (Rahaman et al., Missouri S&T).

Cell proliferation: Total amount of protein in lysates recovered from the cell-seeded trabecular scaffolds were measured with a micro-BCA Protein Assay Kit (Piece Biotechnology, Rockford, IL). The scaffolds were placed in 500 μl of 1% Triton X-100 and the cells were lysed by two freeze-thaw cycles (-80/37 ºC). Sample absorbance values were measured at 550 nm in a BMG FLUORstar Optima plate reader with bovine serum albumin used as a standard for comparison. The amount of protein (**Fig. 24**) showed a nearly linear increase in cell proliferation during the 6 day incubation for the 13-93 and 13-93B1 bioactive glass scaffolds, a finding that complemented the progressive increase in cell density in the live cell/dead cell assays. On the other hand, no significant increase in the amount of protein was found on the 13-93B3 scaffolds, an indication of the inhibiting effects of this scaffold on cell proliferation.

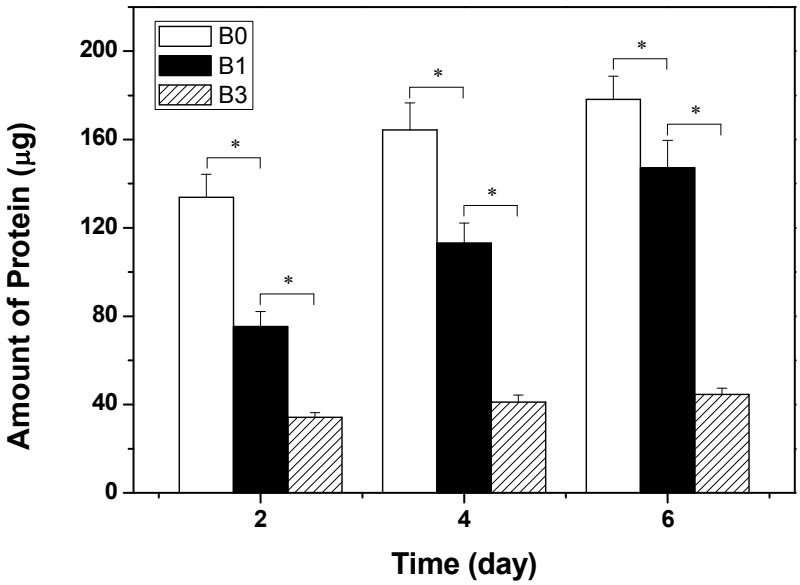

Fig. 24. Ability of 13-93(B0), 13-93B1, and 13-93B3 bioactive glass scaffolds with ability of trabecular microstructure to support proliferation of MLO-A5 cells. Mean ± sd; n = 4. *Significant difference for glass scaffolds with different compositions (p<0.01). (Rahaman, Missouri S&T.)

Alkaline phosphatase activity: The cell-seeded scaffolds were removed at selected time intervals and the cells were lysed using two -80/37ºC cycles. The spectrophotometric measurement of alkaline phosphatase (ALP) in the lysate was conducted with p-nitrophenyl phosphate (p-NPP) substrate as described elsewhere (Sabokar et al., 1994). The ALP activity increased with incubation time for the 13-93 and 13-93B1 scaffolds (**Fig. 25**), an indication that the cells were able to carry out an osteogenic function on these two groups of scaffolds. The much lower and almost stable ALP activity for the 13-93B3 scaffolds during the incubation time was an indication of the poor biocompatibility of the scaffolds.

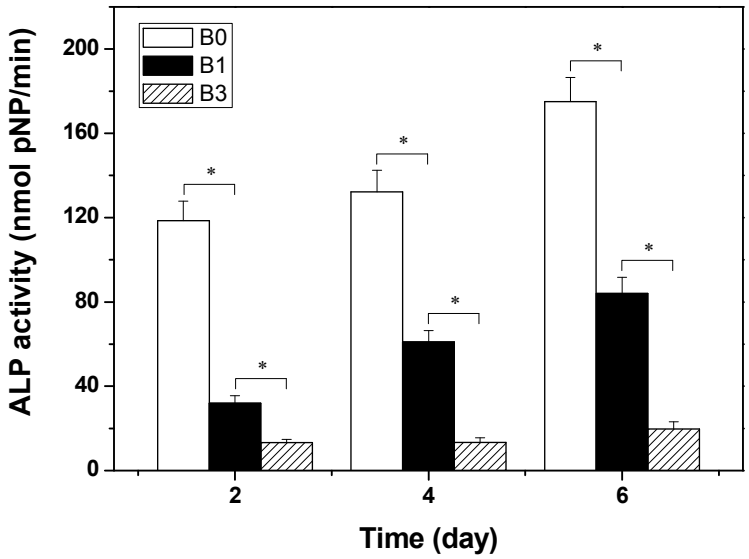

Fig. 25. Ability of 13-93(B0), 13-93B1, and 13-93B3 bioactive glass scaffolds with the trabecular microstructure to support differentiated function of MLO-A5 cells. Mean ± sd; n = 4. *Significant difference for glass scaffolds with different compositions (p<0.01). (Rahaman, Missouri S&T.)

Objective F: *In Vivo* Studies

(F.1) Subcutaneous implantation of bioactive glass scaffolds in rats:

The *in vivo* biocompatibility of the fibrous and trabecular scaffolds and the ability of the fibrous scaffolds to support tissue infiltration were evaluated in a subcutaneous rat implantation model.

Fibrous scaffolds: Scaffolds of 13-93 and 13-93B3 bioactive glass (7 mm in diameter and 2 mm thick), half seeded with 50,000 mesenchymal stem cells (MSCs), half in the as-made condition (unseeded), were placed in subcutaneous pockets in the dorsum of Fisher 344 rats. After six weeks *in vivo*, the scaffolds were removed and processed for histology and SEM analysis.

Assessment of 13-93B3 fibrous scaffolds after implantation for 4 weeks: An as-made scaffold of 13-93B3 was encased in plastic and sectioned as a standard on how the fibers looked prior to implantation. The image (**Fig. 26**) shows several fibers bonded together, and the fibers themselves look rounded. Since the scaffold is comprised of a random fiber orientation, some of the fibers will look elongated as they were cut off center. An H&E stained section of the 13-93B3 scaffold implanted for 4 weeks is shown in **Fig. 27**. The fibers are completely surrounded by soft tissue, and the fibers are no longer solid as in the as-made example above. The fibers have become hollow, and in many cases are filled with tissue.

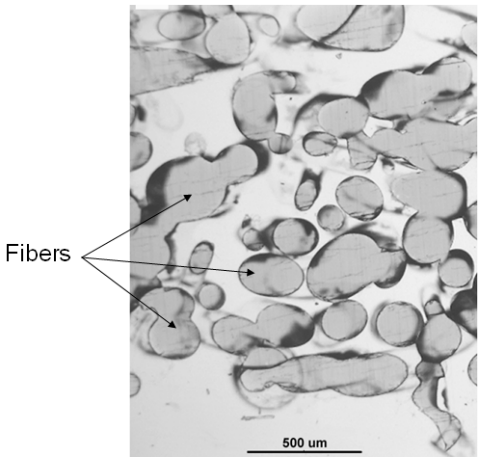

Fig. 26. Optical image of the cross section of an as-prepared 13-93B3 fibrous scaffold. (Day, Missouri S&T)

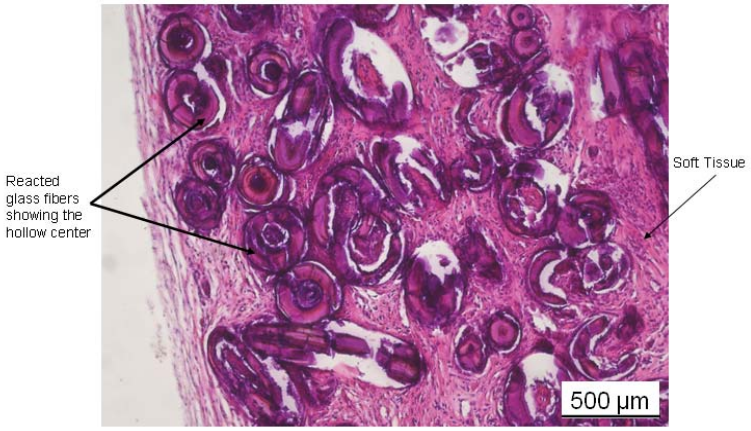

Fig. 27. Transmitted light image of an H&E stained section of 13-93B3 bioactive glass scaffold after implantation for 4 weeks. (Day, Missouri S&T)

Further analysis of the scaffold was done using SEM, as a scaffold was sectioned and imaged. The fibers again are hollow and in many cases filled with soft tissue. The center of a hollow fiber was magnified, and at highest magnification, nano crystals of a material that looked similar to hydroxyapatite (HA) were present (**Fig. 28**).

X-ray diffraction was used to verify that the nano crystals seen in the SEM analysis were in fact HA. **Figure 29** shows the XRD pattern for a 13-93B3 scaffold implanted for 4 weeks as described above, and the crystalline material was identified as HA from the PDF database (card number 72-1243).

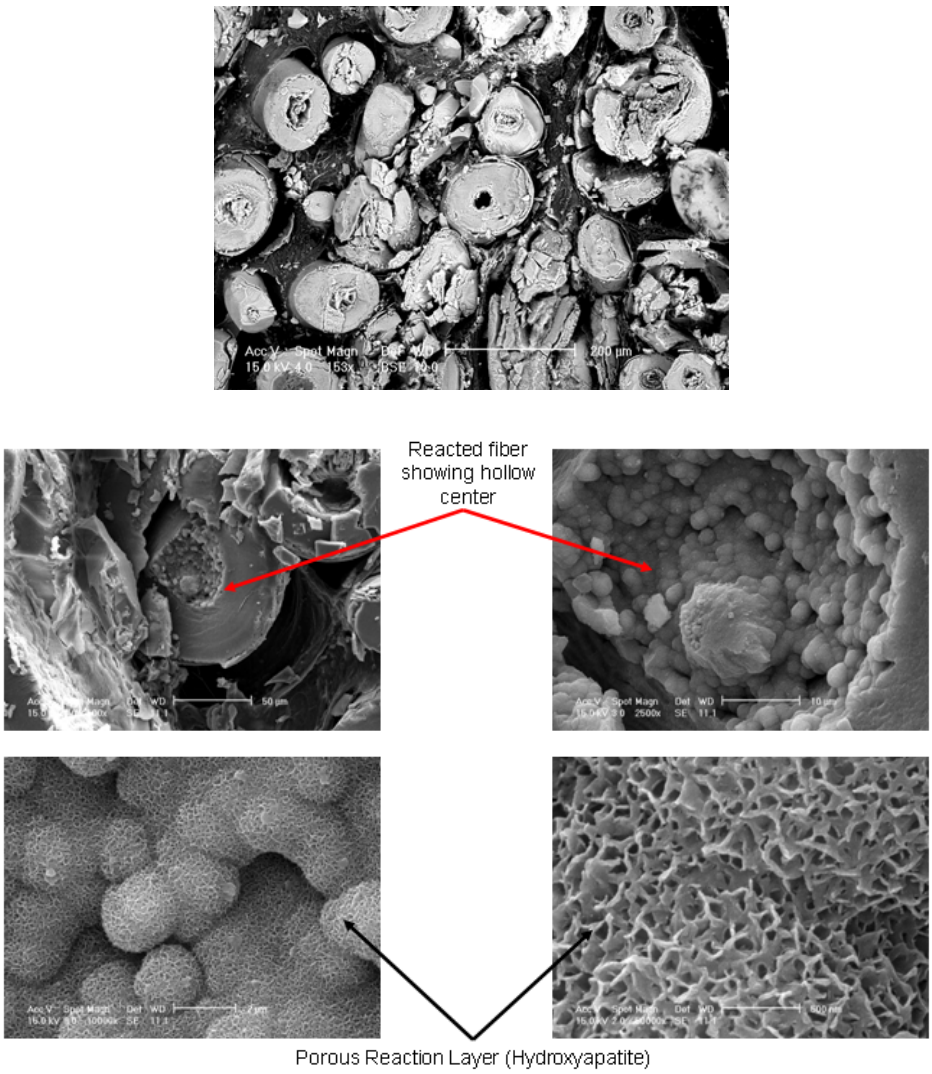

Fig. 28. SEM images of 13-93B3 scaffolds with the fibrous microstructure after subcutaneous implantation for 4 weeks. (Day, Missouri S&T)

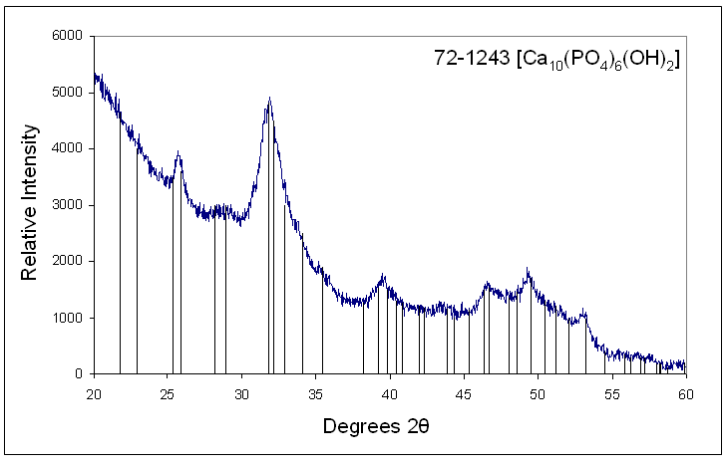

Fig. 29. XRD pattern of 13-93B3 bioactive glass scaffold after implantation for 4 weeks. The pattern of a reference hydroxyapatite (JCPDS 72-1243) is shown for comparison. (Day, Missouri S&T).

Assessment of 13-93 fibrous scaffolds after implantation for 4 weeks: Scaffolds (7 mm in diameter × 2 mm), one group seeded with 50,000 mesenchymal stem cells (MSCs), and another group in the as-made condition (unseeded), were placed in subcutaneous pockets in the back of Fisher 344 rats and incubated for 3 and 4 weeks. Upon extraction, all the scaffolds were completely filled with soft tissue with several areas containing visible blood vessels penetrating the scaffolds (**Fig. 30**).

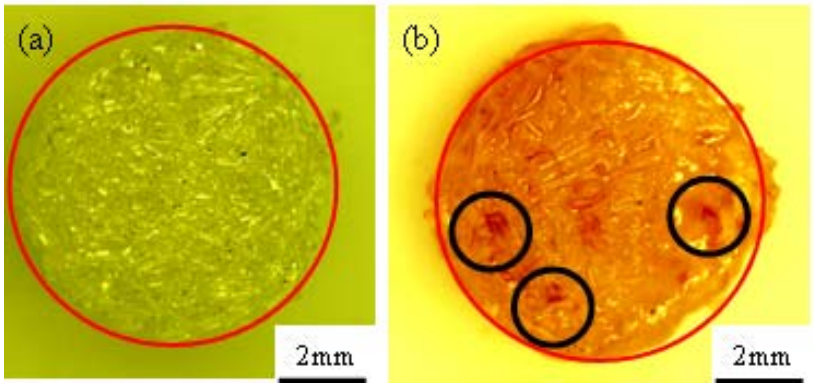

Fig. 30. Optical micrographs of 13-93 bioactive glass scaffolds with the fibrous microstructure (a) as-made scaffold; (b) after seeding with MSCs and implanted for 4 weeks in subcutaneous pockets in the dorsum of Fisher 344 rats. The red circle is 7 mm in diameter and denotes the starting diameter of each scaffold (Day, Brown; Missouri S&T).

Subsequent sectioning and staining of the scaffolds identified both soft and hard (bone) tissue in the MSC-seeded scaffolds, whereas the as-made scaffolds only contained soft tissue (**Fig. 31**).

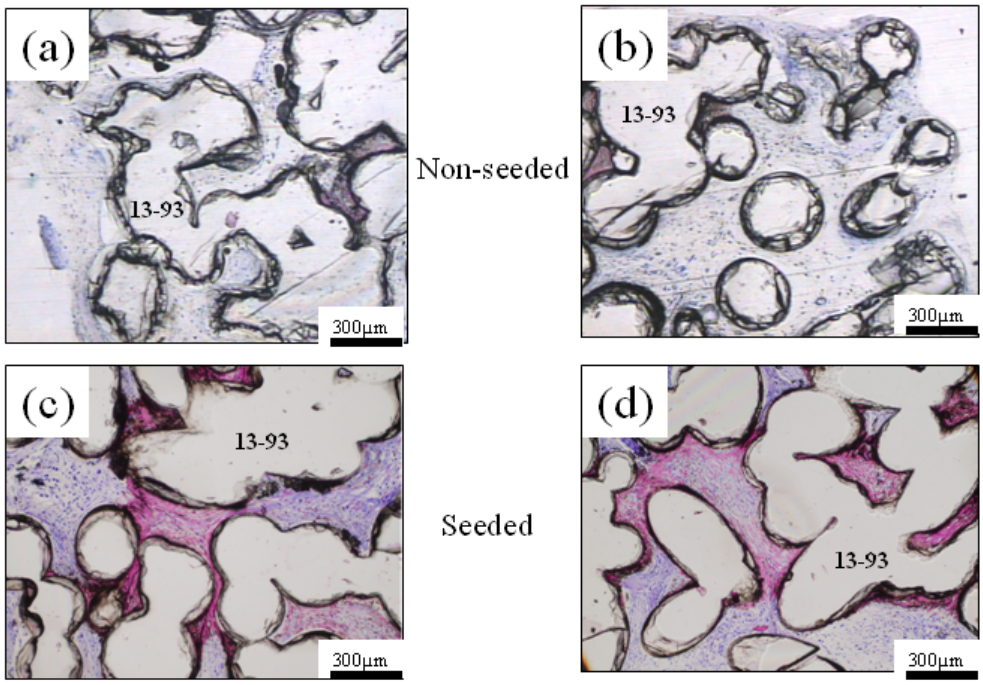

Fig. 31. Optical micrographs of the cross section of 13-93 bioactive glass scaffolds with the fibrous microstructure after subcutaneous implantation for 3 weeks (a), (c), or 4 weeks (b), (d). Blue tissue represents soft tissue, whereas red represents hard (bone) tissue. (Day, Brown; Missouri S&T)

Back-scattered electron (BSE) images taken in the SEM (**Fig. 32**), coupled with energy-dispersive X-ray (EDS) analysis of sections of the MSC-seeded scaffolds, confirmed that the areas stained positive for bone was a calcium phosphate material, with a composition similar to that of stoichiometric hydroxyapatite (HA).

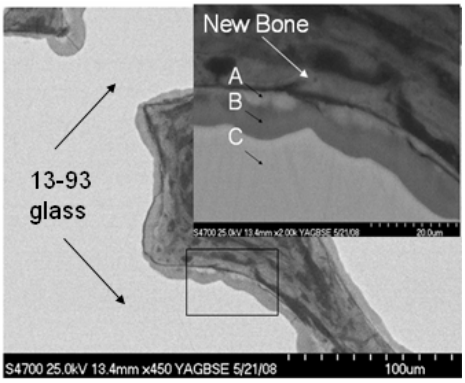

Fig. 32. SEM back-scattered electron image of a section of a MSC-seeded scaffold after implantation for 4 weeks. The magnified view (inset) shows new bone growing adjacent to 13-93 glass fiber. The area labeled A is a calcium phosphate-rich region similar in composition to HA, area B is a silica-rich region, and area C is the unreacted 13-93 glass. (Day, Missouri S&T).

Trabecular scaffolds:

Figure 33 shows the gross appearance of a MSC-seeded trabecular scaffold (13-93) after subcutaneous implantation for 4 weeks in the dorsum of Fisher 344 rats. A calcium phosphate layer, with a Ca/P ratio corresponding to that of hydroxyapatite (HA), ~20 μm thick, was formed on the surface of the 13-93 bioactive glass of the trabecular scaffold (**Fig. 34a, 34b**).

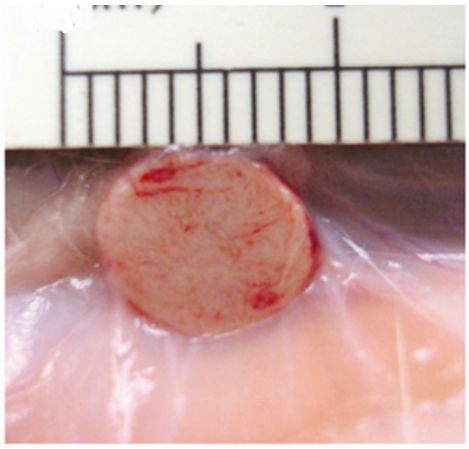

Fig. 33. Gross appearance of 13-93 bioactive glass scaffold after implantation for 4 weeks in subcutaneous pockets in the dorsum of Fisher 344 rats. (The scale is in mm.) (Rahaman, Missouri S&T).

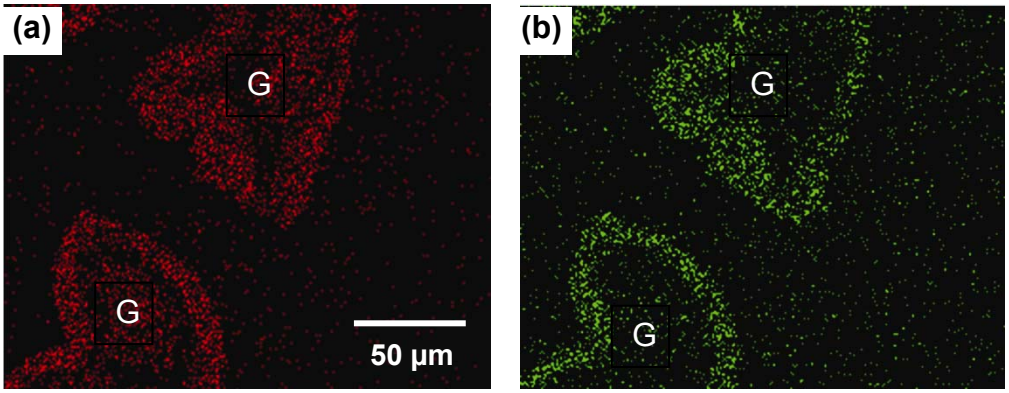

Fig. 34. X-ray maps for (a) Ca(K) and (b) P(K), respectively, of a 'trabecular' scaffold (G), showing a hydroxyapatite-type layer (~20 μm thick) formed on the glass surface (Rahaman, Missouri S&T).

Sections of trabecular scaffolds (13-93, 13-93B1, and 13-93B3), 6 weeks post implantation, were stained with hematoxylin and eosin (H&E), toluidine blue, and Goldner's trichrome. Transmitted light images (**Fig. 35**) showed abundant tissue infiltration into the scaffolds. The intra-glass stroma in 13-93B3 appeared to be less fibrillar when compared to 13-93 and 13-93B1, while the stroma in 13-93B1 appear to be more abundant than in 13-93.

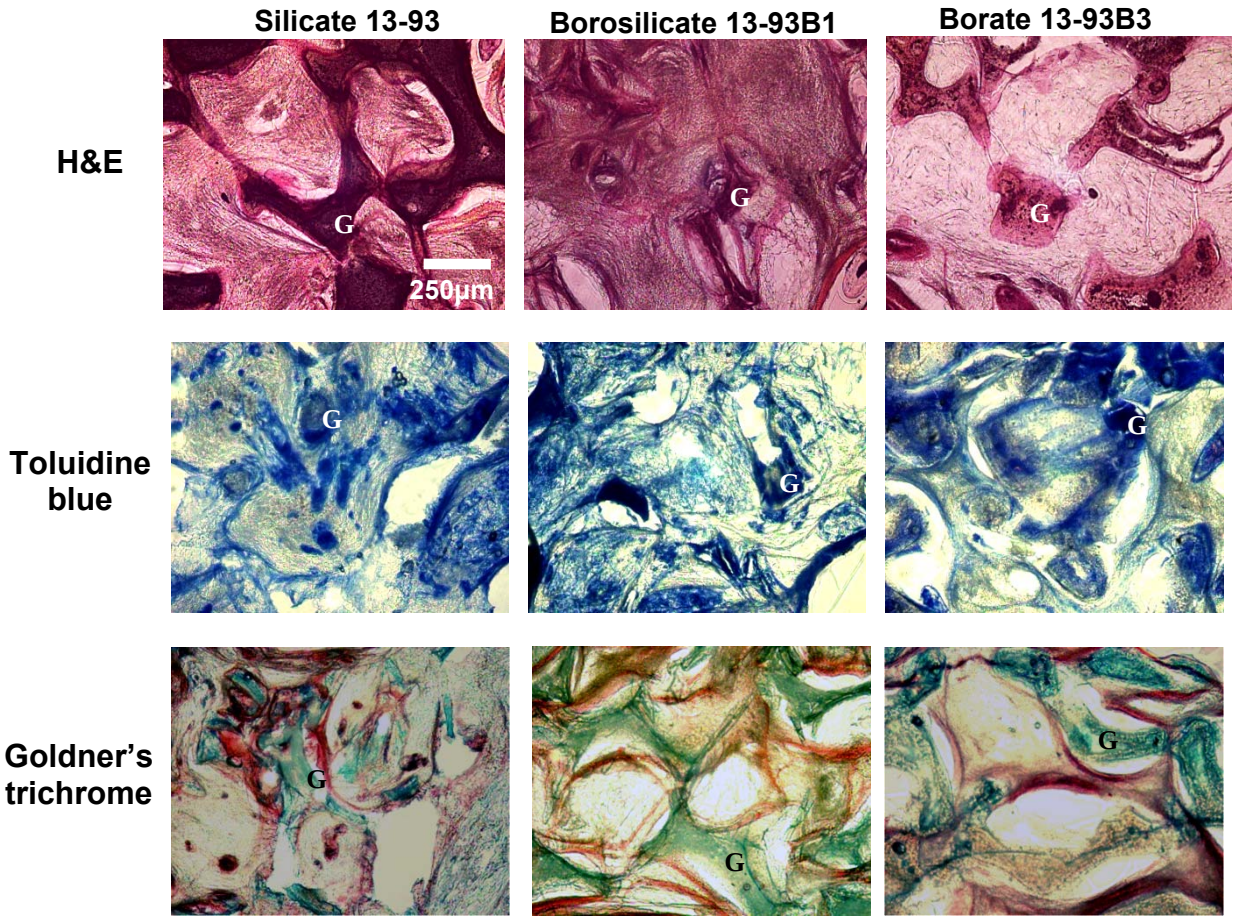

Fig. 35. Transmitted light images of H&E, toluidine blue, and Goldner's trichrome stained sections of trabecular scaffolds with the 13-93, 13-93B1, and 13-93B3 composition after subcutaneous implantation for 6 weeks in the dorsum of Fisher 344 rats. (All images have the same magnification as that for H&E stained 13-93; G denotes the scaffold.) (Rahaman, Missouri S&T).

(F.2) Toxicity of borate (13-93B3) glass scaffolds

Histological analyses showed no adverse effects resulting from subcutaneous implantation of borate bioactive glass (13-93B3) scaffolds in rats. Five groups of rats were evaluated: control (without borate bioactive glass scaffolds), and animals implanted subcutaneously with 4, 8, 12, and 16 scaffolds (n=4 per group), to determine the effect of boron release from borate bioactive glass (13-93B3) scaffolds on the kidney or liver. The scaffolds (70 mg) were implanted for 4 weeks. Based on previous subcutaneous implantation experiments, this implantation time was long enough for the scaffolds to completely react and convert to a hydroxyapatite-like material *in vivo*. After the animals were sacrificed, a kidney and a lobe of the liver were removed from each animal, and sections of each organ were cut and stained with hematoxylin and eosin (H&E). The sections were sent for blinded histological evaluation to Charles River Labs LLC (Massachusetts), a commercial company that provides research and laboratory animal support services. The results from each animal are shown in **Table II**.

No histological findings were discovered in the liver of any group (**Fig. 36**). The kidney had only minor incidental changes often seen in adult rats. No severe toxicity was reported indicating that the bioactive borate glass caused no tissue damage to the kidney or liver. The boron release, calculated as boric acid for comparison with published literature, was at most ~125 mg/kg/day. This level was below the maximum published value for safe boric acid consumption by an adult Sprague Dawley rat (~160 mg/kg/day), therefore no major histological changes was expected. The total amount of glass in the rats (300 g) implanted with 16 scaffolds was ~1.12g. In a human weighing 100 lbs, this would be equivalent to about 170 g of glass. This amount of glass is approximately one order of magnitude higher than the amount required for any current applications using bioactive glass. **From the histological findings to date, it is concluded that borate-based bioactive glass (13-93B3) should be considered safe for mammalian and human use.**

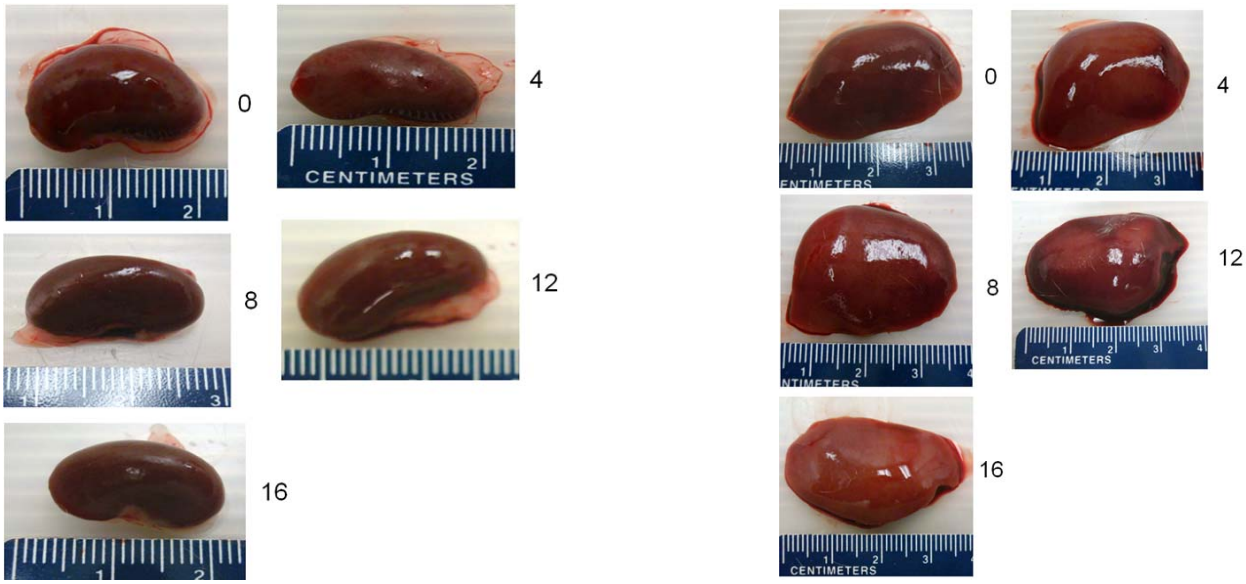

Fig. 36. Photographs of a representative left kidney (left) and liver (right) recovered after four weeks from rats implanted with up to 16 13-93B3 scaffolds (70mg each): control (0), 4, 8, 12, and 16 scaffolds respectively. There were no spots of color differences in any of the kidney and the sizes of the kidney were all the same. No lesions or discoloring was observed with any of the livers as compared to the control and the size of each liver was similar. (Day, Missouri S&T)

Table II.

Histological Findings for Sprague Dawley Rats Implanted with 13-93B3 Bioactive Glass Fiber Scaffolds (70mg) for Four Weeks

# of Scaffolds per Animal	16	16	16	16	12	12	12	12	8	8
Tissue Finding										
Kidney	+	+	+	-	+	+	-	+	+	+
Degeneration, tubular	1M	1M	-	-	-	-	-	-	1M	-
Protein casts, tubular	1M	1M	1M	-	-	1M	-	-	1M	1M
Nephrocalcinosis	1M	-	-	-	1F	-	-	1M	1F	-
Liver	-	-	-	-	-	-	-	-	-	-

# of Scaffolds per Animal	8	8	4	4	4	4	Control	Control	Control	Control
Tissue Finding										
Kidney	-	+	+	+	+	+	-	+	+	+
Degeneration, tubular	-	-	-	-	1M	1M	-	-	-	-
Protein casts, tubular	-	1M	1M	1M	1M	1M	-	1M	1M	1M
Nephrocalcinosis	-	-	-	-	-	-	-	-	-	-
Liver	-	-	-	-	-	-	-	-	-	-

Key: - =negative/no significant finding; + = positive/finding present; 1 = minimal severity; 2 = mild severity; 3 =moderate severity; 4 = marked severity; F = focal; M = multifocal; D = diffuse.

(Toxicity report provided by was provided by Charles River Labs LLC, Massachusetts).

(F.3) Implantation of Different Bioactive Glass Scaffolds into Bony Defects in Rats

The bone formation, angiogenesis and hydroxyapatite conversion of the glasses were evaluated in a critical-sized rat calvarial defect model.

Materials and Methods

Surgical Procedure: Fourteen 12-week old Sprague-Dawley rats underwent surgery in which bilateral critical-sized calvarial defects were created. The rats were anesthetized with 3.5% isoflurane and ketamine/dexdomitor (75 mg/0.25 kg body weight), their heads were shaved and scrubbed with sterile gauze soaked with betadine and rinsed with sterile water three times. A one centimeter incision was made along the cranial midline, the calvarium was exposed, and two 4 mm diameter defects were created in the parietal bone with a dental bur under irrigation (**Fig. 37**).

Each defect was assigned to one of five treatment groups: the defect was implanted with bioactive glass scaffolds: (1) 13-93, (2) 13-93B1, (3) 13-93B3, each in the form of a disk measuring 4 mm in diameter and 2 mm thick, (4) 45S5, as positive control, implanted as packed particles, or (5) the defect was left empty for negative control. The borosilicate and borate glasses were derived from the silicate 13-93 glass by partially or fully replacing the silica with boron oxide. The compositions of the four glasses are given in **Table I**. The scaffolds, with a "fibrous" microstructure similar to that shown in **Fig. 3**, were provided by Dr. Delbert Day at the Department of Materials Science and Engineering, and Center for Bone and Tissue Repair and Regeneration, Missouri University of Science and Technology, Rolla, Missouri.

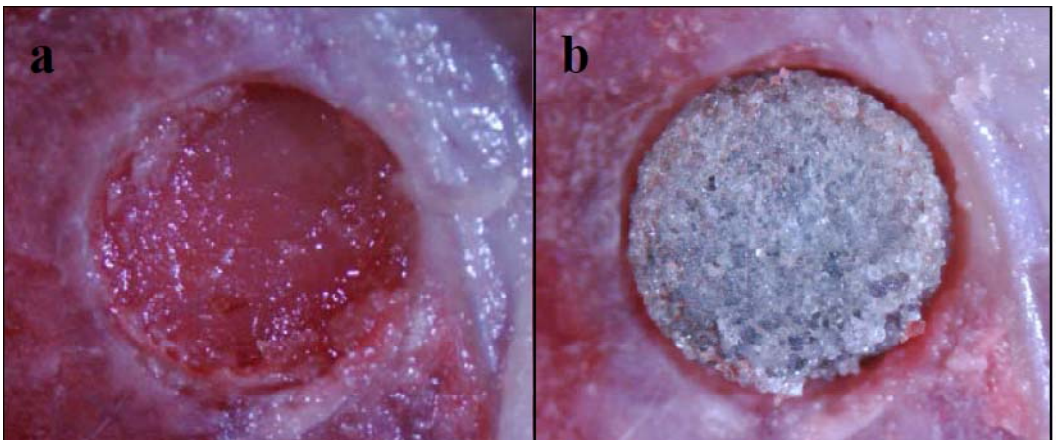

Fig. 37. (a) 4mm diameter defect created in parietal bone, (b) defect filled with bioactive glass.

Micro CT examination: All rats were scanned at one week post surgery to serve as baseline and then scanned every three weeks up to 12 weeks. The images of defects implanted with different glass scaffolds for 12 weeks are shown in **Fig. 38.** New bone formed on the top and bottom of the bioactive glass scaffolds. The most area of the bottom of scaffold was covered by new bone in glass 45S5, 1393 and 1393B1. In 1393B3, the new bone completely covered the bottom surface. The midsection showed that the glasses integrated with bone tissue.

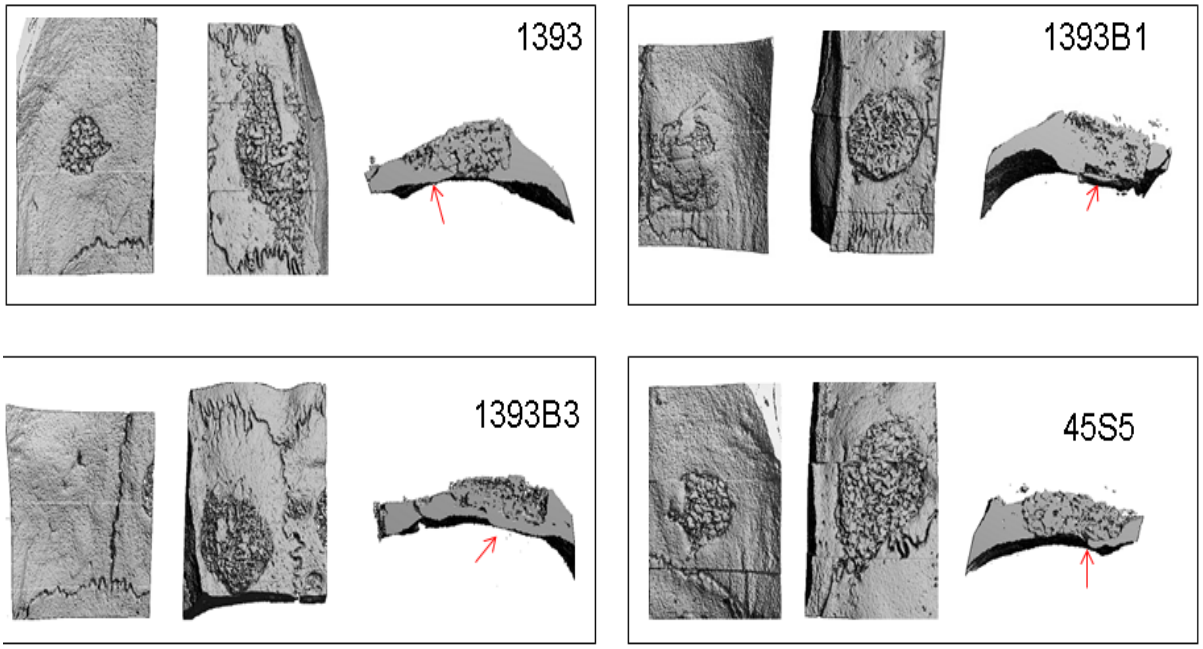

Fig. 38. Micro CT images of critical-sized rat calvarial defects implanted with the glass 45S5, 1393, 1393B1 and 1393B3 at 12 weeks post surgery. The arrows point to the new bone.

Histologic Processing: The rats were sacrificed at 12 weeks post-surgery by CO_2 asphyxiation. Calvarial samples including the surgical sites were removed and cut into approximately equal halves. Half of the sample was decalcified with 14% EDTA, fixed in 10% buffered formaldehyde, dehydrated in ethanol, and embedded in paraffin. The other half of the sample was left undecalcified, fixed, dehydrated, and embedded in methylmethacrylate plastic. Paraffin sections were prepared with a rotary microtome (Microm HM315, Microm International, Thermo Fisher Scientific, Walldorf, Germany) to a thickness of five micron, while plastic sections were prepared with a rotary microtome (Microm HM355S, Microm International) to a thickness of 8-10 micron. All sections were placed on Thermo Scientific Superfrost Excell Adhesion Slides (Thermo Scientific, Kalamazoo, MI) coated with Haupt's Adhesive (Dorn and Hart Microedge, Inc, Villa Park, IL).

Decalcified sections of each sample were stained according to protocol with Hematoxylin and Eosin Phloxine Orange G. The Phloxine and Orange G are added to broaden the range of red/pink stained by Eosin. First, slides were placed in three 5-minute changes of xylene, in two changes of 100% ethanol, each for one minute, then into 95% and 70% EtOH, each for one minute, and rinsed through two changes of tap water. Slides were then placed in Hematoxylin (Lot 95400, Richard Allen Scientific, Kalamazoo, MI) for four minutes. Slides were rinsed through three changes of tap water, dipped twice in 1% acid alcohol, and again rinsed through three changes of tap water before being placed in 1x PBF (phosphate buffered saline), and rinsed through two changes tap water. Slides were placed in 95% EtOH for 30 seconds before being put in Eosin Phloxine Orange G for 30 seconds [500 mL Eosin (Lot 31296CJ, Sigma Aldrich, St. Louis, MO), 37 mL 1% Phloxine B (Lot 077K1855, Sigma-Aldrich), 16 mL 2% Orange G (Lot 028K3744, Sigma-Aldrich)]. Slides were dehydrated through 30 seconds each of 95% and 100% EtOH, then through two one-minute changes of 100% EtOH before being placed in three changes of xylene, each for two minutes. Coverslips (Mercedes Medical, Sarasota, FL) were mounted with Permount Toluene Solution (Lot 096403, Fisher Scientific).

Each sample also had sections stained Periodic Acid Schiff with 1% Light Green counterstain. PAS stains carbohydrates in tissue and the light green counterstain is picked up well by red blood cells, resulting in purple-stained blood vessels and green-stained red blood cells. To make the Schiff Reagent, 800 mL of water was heated to boiling, removed from heat, and 4.0 g Basic Fuchsin (Hydrochloride, Cat#150423, MP Biomedicals LLC, Solon, OH) was added. The solution was heated again to boiling, allowed to cool, and was filtered. 80 mL of 1 N Hydrochloric acid was added, ensured the solution had cooled completely, and then 4.0 g Sodium metabisulfite (Lot 01920PW, Aldrich Chemical Company, Inc, Milwaukee, WI) was added. The solution was left

to stand overnight, after which it had turned light amber. Two grams of activated charcoal were added and the solution was shaken for one minute, filtered until clear, and stored in the refrigerator. Slides were deparaffinized with xylene and hydrated to distilled water. They were placed in 0.5% Periodic acid (Lot 1383178, Sigma-Aldrich) for 5 minutes, rinsed through three changes distilled water, and placed in Schiff 23 Reagent for 15 minutes. Slides were then left in tap water for 10 minutes to develop full color, after which they were counterstained for 30 seconds in 1% Light Green SF (Fisher Scientific Cat#03382, CAS#5141-20-8, Fair Lawn, NJ), rinsed well with distilled water, dehydrated with 95% EtOH and 100% EtOH, cleared with three changes of xylene, and coverslips were mounted with Permount.

The undecalcified sections were stained von Kossa with 5% silver nitrate. The silver reacts with anions of the calcium salts, so in the case of calcium phosphate it is the phosphate that binds the silver. Bright light reduces the silver salt, resulting in a black stain indicating the presence of calcium phosphate, and pink stained soft tissue from the Eosin counterstain. First, the slides were deplasticized using four changes of Ethylene Glycol Monoethyl Ether Acetate (Lot 090684, Fisher Scientific), 10 minutes each. The slides were checked after the last change of EGMEA by dipping in 100% EtOH, if any slides showed signs of MMA residue they were placed back in EGMEA until clear. The slides were then placed in two changes 100% EtOH and rehydrated through 95% EtOH to distilled water. Glass containers to hold the slides were bleached and distilled-water rinsed because introduction of any metal would contaminate the silver nitrate. Slides were placed in filtered 5% Silver nitrate (Lot A0284428, Acros Organics, Thermo Scientific) and placed under a 100W light bulb for 90 minutes (waited until the tissue turned black). The slides were rinsed in two changes of distilled water, rinsed with 5% Sodium thiosulfate (Lot 71K2206, Sigma-Aldrich) for 5 minutes, and again rinsed in distilled water. They were then placed in 30 seconds each of 70% and 95% EtOH, placed in Eosin 30 seconds, and quickly rinsed with 95% EtOH before going through three changes 100% EtOH, two for 30 seconds and the last for one minute. They were put through three changes of xylene, for one minute each, and then coverslips were mounted with Permount.

Histomorphometric Analysis: Histomorphometry was carried out using a light microscope (Eclipse E800, Nikon Instruments Inc, Melville, NY) with a color video camera (Model DXC-390P, Sony, Tokyo, Japan) attached. The live image was displayed on a computer and analyzed with a bone histomorphometry software program, Osteomeasure (Version 2.2, Osteometrics Inc, Atlanta, GA). For histomorphometric analysis of percent new bone growth within the defect, the sections with H&E staining were used. Bone morphology was used to demarcate the edge of the defect, with the presence of lamellar and woven bone indicating original and new bone, respectively (**Fig. 39a**). Viewed at 4x magnification, the entire defect area was measured from the edge of the original calvarial bone, including entire glass scaffold and tissue within, to the other edge of the old bone. The new bone growth within this area was then outlined (**Fig. 39b**) and the Osteomeasure software calculated the areas to determine the amount of newly formed bone, expressed as a percentage of the total defect area.

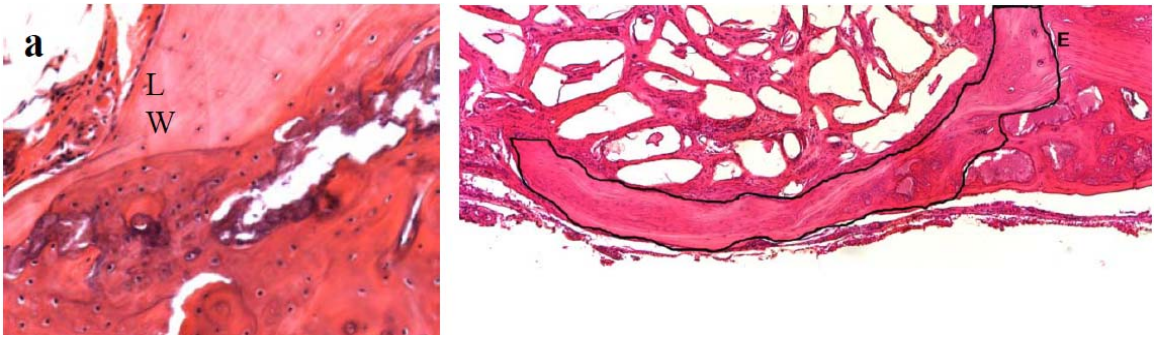

Fig. 39. Light microscopy images of H&E stained sections of the scaffolds in calvarial defect; (a) 20x view demonstrating difference between lamellar (L) and woven (W) bone, (b) 4x view demonstrating how new bone was outlined, where E indicates the edge of the defect.

Quantitation of blood vessel area within the defect was performed using the sections stained by PAS, which results in purple-stained blood vessels, with counterstaining yielding green red blood cells, as shown in **Fig. 40a**. Viewed at 20x, each scaffold was scanned using the template shown in **Fig. 40b** to acquire six regions of

interest, within which the blood vessels were outlined. All six areas were combined by the Osteomeasure software to determine a total blood vessel area, which was expressed as a percentage of the area of the selected regions.

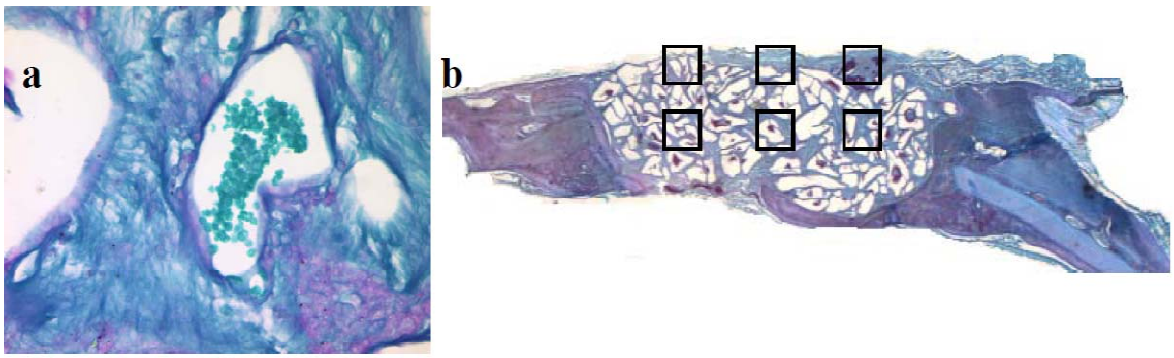

Fig. 40. Light microscopy images of PAS stained sections of scaffold within calvarial defect. (a) 40x view of blood vessel with red blood cells inside, (b) 1x view of glass scaffold defect area with template used for determining areas of quantitation

Quantitation of von Kossa-positive area was performed using imageJ software. 4x images of the von Kossa stained sections were used (**Fig. 41a**). Images were converted to 8-bit (**Fig. 41b**) and a threshold was adjusted to measure only the black-stained areas of the image (**Fig. 41c**), which yielded the black area fraction as a percentage of the total area. von Kossa will stain calcium phosphate in both bone and hydroxyapatite, so in order to determine the percentage area taken up only by the glass, the von Kossa positive percentages were averaged for each sample, then the percentages of new bone growth (previously determined by the H&E sections) were subtracted.

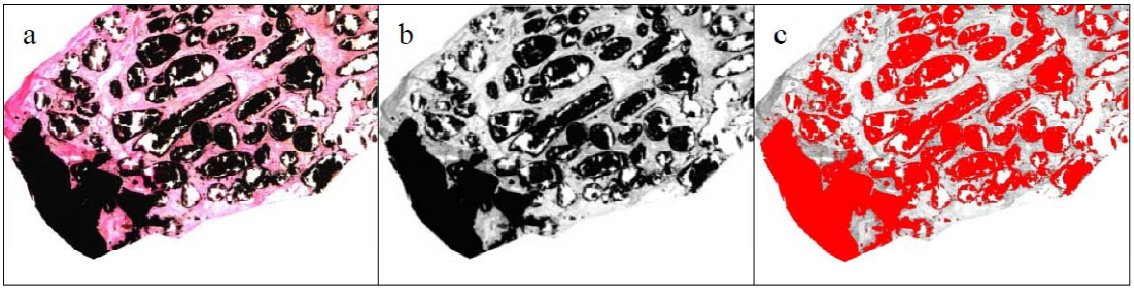

Fig. 41. Light microscopy images of von Kossa stained images taken at 4x magnification. (a) original image, (b) image converted to 8-bit, (c) image with threshold applied.

Data Analysis

Average area values for new bone, blood vessel, and von Kossa-positive areas were analyzed using one-way analysis of variance (ANOVA) with Tukey-Kramer Multiple Comparisons post-hoc test. A p-value less than 0.05 was considered statistically significant. Sample size was five for each treatment group.

Results

Bone regeneration: With all implanted bioactive glasses, the majority of new bone growth was seen along the edges of the defect (adjacent to old bone), with many samples demonstrating bone bridging across the defect along the bottom (dura side). Samples from all four glasses demonstrated bony “islands” within the scaffold. The positive control, 45S5, had an average new bone growth of 12.4% ± 1.2 (SEM) within the defect, while the 13-93 silicate glass had 8.5% ± 1.6, the 13-93B1 borosilicate glass had 9.7% ± 1.8, and the greatest amount of bone growth was observed in the defects implanted with the 13-93B3 borate glass, 14.9% ± 1.9 (**Fig. 42**). The bone growth within the defect implanted with B3 was significantly higher ($p = 0.04$) than the 13-93 silicate glass. There was no significant difference between 13-93B3 and 45S5, but new bone growth for B3 was approximately 13% higher than 45S5.

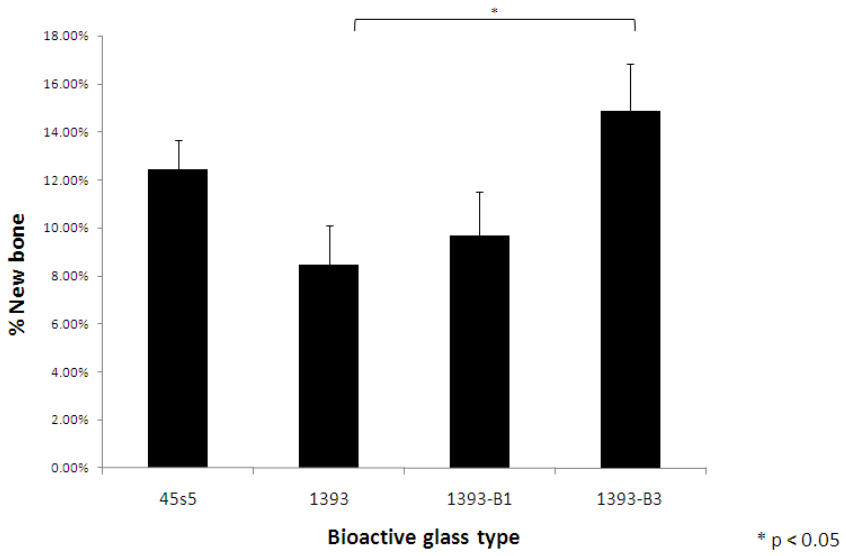

Fig. 42. Percent new bone regeneration in rat calvarial defects implanted with different bioactive glass scaffolds, where *p< 0.05.

Blood vessel area: For all of the implanted bioactive glasses, blood vessel infiltration was observed throughout the defect. From personal observation, it was noted that the highest concentration of blood vessels was along the bottom (dura side) of the defect. Of the four bioactive glasses, 45S5, the positive control, had the highest percentage of blood vessel area within the defect, at 3.8% ± 0.29. This was significantly higher (p = 0.009) than all three experimental glasses. There was no trend among 13-93, 13-93B1, and 13-93B3 in blood vessel area, as values were 2.0% ± 0.3 for 13-93 silicate glass, 2.4% ± 0.44 for 13-93B1 borosilicate glass, and 2.2% ± 0.64 for 13-93B3 borate glass (**Fig. 43**).

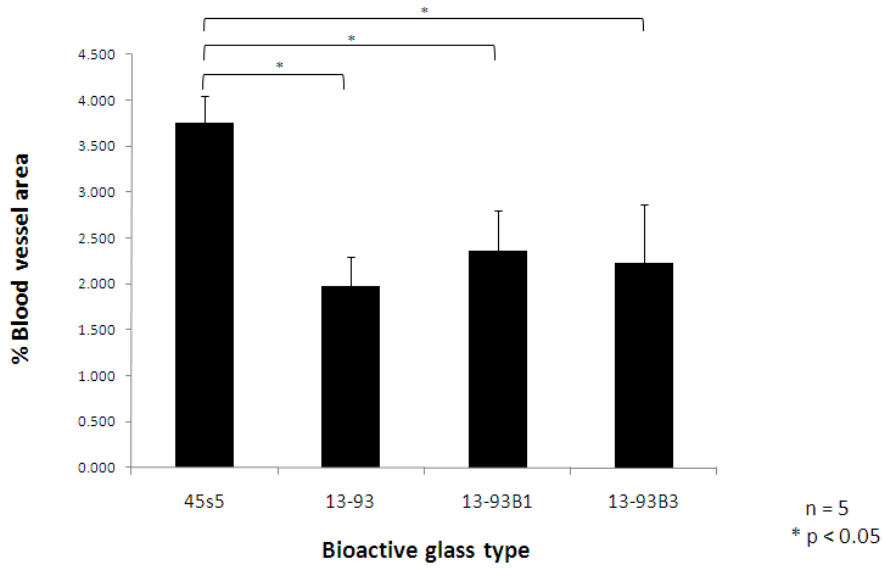

Fig. 43. Percent blood vessel area in rat calvarial defects implanted with different bioactive glass scaffolds, where *p<0.05.

von Kossa-positive area: The von Kossa-positive areas indicate the presence of calcium phosphate, which is present in mineralized bone. We assume the von Kossa-positive staining within the glass particles can be attributed to calcium phosphate in the hydroxyapatite-like layer. Total von Kossa-positve area within the defect was 30.7% ± 3.0 for 45s5, the positive control, 34.1% ± 4.3 in the 13-93 silicate glass, 39.2% ± 2.9 in the 13-

93B1 borosilicate glass, and highest in the 13-93B3 borate glass, 45.3% ± 5.0. Percent von-Kossa positive area was significantly higher (p = 0.04) in the 13-93B3 glass than in 45s5, but there was a visible trend of increased von-Kossa positive area with increased boron oxide content of the glasses (**Fig. 44**).

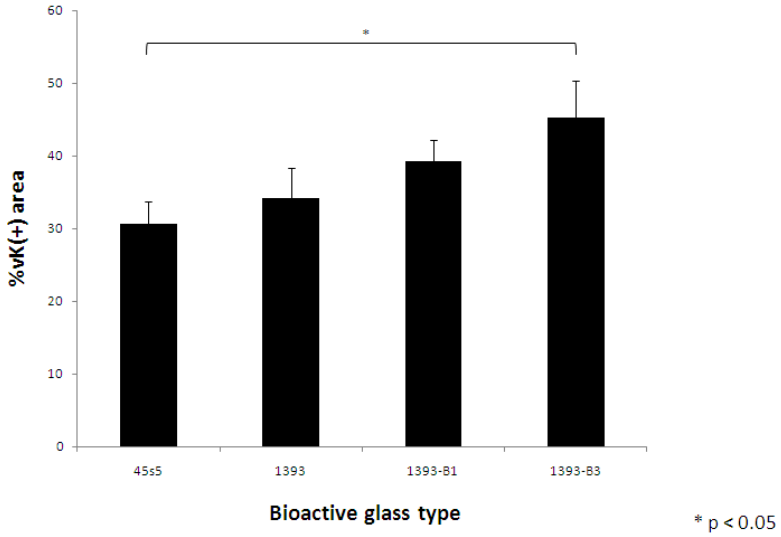

Fig. 44. Von Kossa-positive area in rat calvarial defects implanted with different bioactive glass scaffolds, where *p<0.05.

To evaluate how much of the von Kossa-positive area was attributed to the glass alone, the values of new bone regeneration (see Figure 5) were subtracted from the total von Kossa-positive values. The difference could be attributed to the glass conversion to hydroxyapatite. Percent von Kossa-positive area for the glass, or estimation of hydroxyapatite conversion, was 18.7% ± 3.2 in the 45S5 glass, 25.4% ± 3.1 in the 13-93 silicate glass, 29.5% ± 1.3 in the 13-93B1 borosilicate glass, and 30.1% ± 3.2 in the 13-93B3 borate glass. Estimated hydroxyapatite conversion was significantly higher (p = 0.014) in the B1 and B3 glasses than in the 45S5 positive control (**Fig. 45**).

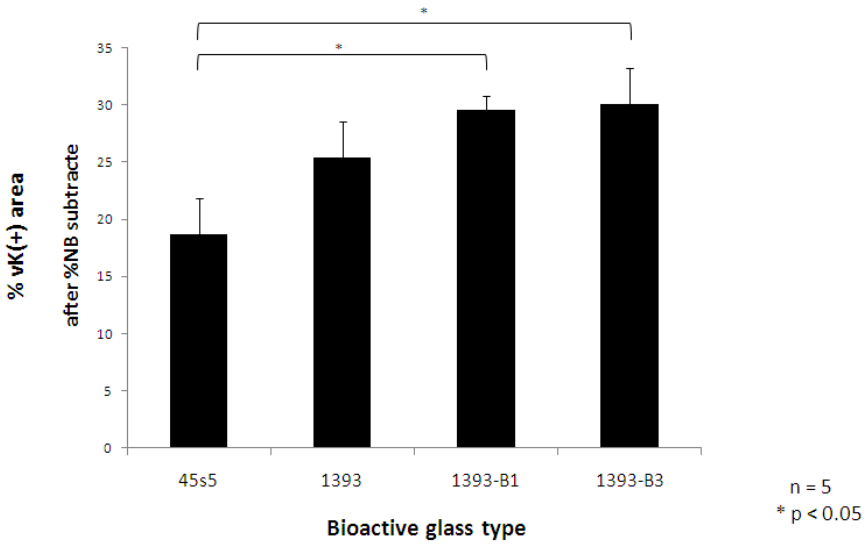

Fig. 45. Estimation of hydroxyapatite conversion in bioactive glasses implanted in rat calvarial defects, where *p<0.05.

The calvarial defects left empty all demonstrated bone growth along the edges of the defect with connective tissue bridging across the remainder of the gap. The percentage area of new bone growth for the empty defect

was 31%. This value cannot be used as negative control due to the fact that the total defect area was significantly less than that of the implanted glasses. There was a nearly two-fold difference in defect area between the empty and implanted defects due to the scaffolds being nearly twice as thick as the calvaria itself. Due to this, it can be inferred that the average new bone growth within the empty defects was approximately 15%; still relatively high in comparison to the treatment glasses (see **Fig. 42**) due to the fact that the new bone growth at the edges of the defect was not impeded by the glass particles. Blood vessel infiltration was also observed within the connective tissue of the empty defect, with its blood vessel area only 1.44%.

Discussion

We hypothesized that increased boron oxide content of bioactive glasses would result in increased bone growth, blood vessel content, and hydroxyapatite conversion. Our hypothesis was validated by the results of new bone and hydroxyapatite conversion, however the blood vessel results were contradictory. Among the 13-93 glasses, new bone growth within the defect increased with increasing boron oxide content of the glass, with the 13-93B3 borate glass with the most observed bone growth. This result indicates that replacing the silica oxide with boron oxide significantly increases the amount of neoformed bone in a critical-sized rat calvarial defect. Though not significant, the 45S5 glass did demonstrate more bone growth than the 13-93 glass which is of similar composition. From observation, most of the new bone was along the edge of the defect, though several samples showed new bone bridging across the defect, most noticeably along the bottom (dura side) of the defect. This may be where 45S5 had an advantage over 13-93, as it was observed that 45s5 had more bone growth bridging across the defect. If not due to compositional difference, this may be due to the particulate nature of the glass, in that the new bone can grow across the defect implanted with particulate glass more easily as opposed to the scaffold structure of the 13-93. However, this difference could be overcome by the effect of the added boron oxide in the 13-93B1 and 13-93B3 glasses, as they both demonstrated bridging across the defect.

As new bone is growing within the defect, it requires vasculature present to keep it nourished. It follows then, that one would expect more blood vessels in the defects with the most bone growth. The results of this study did not support this hypothesis; instead we observed the most blood vessel area in the 45S5 glass, and no trend among the 13-93, 13-93B1, and 13-93B3 glasses. It may be that the different compositions of the glasses have no effect on angiogenesis, and that the particulate nature of 45S5 has an advantage over the scaffold glasses in that the blood vessels are able to more easily penetrate the packed particles of the 45S5 glass.

We utilized the von Kossa staining as a means to identify the presence of calcium phosphate within the defects, indicating mineralization and thus the presence of bone and hydroxyapatite. We expected the results to follow the hypothesis that the glasses with higher boron oxide content would be converting to hydroxyapatite faster, and would therefore have higher amounts of calcium phosphate. Our results did support this hypothesis, in that the total von Kossa-positive areas determined were significantly higher in the borate glass. Once the values for percent new bone growth within the defect were subtracted from the total von Kossa-positive values, the 13-93B1 and 13-93B3 bioactive glasses had nearly identical values of estimated hydroxyapatite conversion. These results indicate that both B1 and B3 had already converted, as these rats were sacrificed at 12 weeks post surgery, and our results give no evidence for the rate of hydroxyapatite conversion. We speculate that the borate glass did convert faster than the other glasses, but that both the 13-93B1 and 13-93B3 glasses were converted by the time of analysis. Our results indicate that the 45S5 and 13-93 glass were still incompletely converted to hydroxyapatite at 12 weeks.

Our results are consistent with the work reported by Liu et al. 2009, in which it was demonstrated that 45S5 and 13-93 convert slowly and incompletely to hydroxyapatite. It has also been shown with borosilicate and borate glasses that hydroxyapatite conversion rate increases with the boron content (Huang et al. 2005, Yao et al. 2006, Fu et al. 2010); our *in vivo* von Kossa results are consistent with these findings as well. Based on the work of Gorustovich et al. 2006, in which it was shown that adding boron oxide to 45S5 results in significantly higher neoformed bone tissue around the glass particles, we can infer that our bone regeneration results are due to the boron oxide content because the borate glass had the highest percentage of new bone growth. Limitations of this study include the use of 45S5 as a positive control, due to the difference in structure of the implanted glasses; and also the use of scaffolds which were thicker than the calvaria itself, which resulted in the lack of comparison to a negative control. We also recommend examining the possible toxic effects of boron

more closely, as there could have been neurological damage to the brain underlying the defect at the cellular level, though the authors did not observe any gross neurological signs of toxicity.

Future studies with these bioactive glasses could include examining the scaffolds over a longer period of time to evaluate bone growth and scaffold conversion, biomechanical testing to evaluate strength of the scaffolds *in vivo*, and testing these glasses in other types of bone such as long bone, spine, and mandible. Future studies could also attempt to enhance the rate and amount of bone regeneration by coating the scaffolds with growth factors (TGF, FGF, IGF, BMPs), seeding them with bone marrow-derived mesenchymal stem cells, or adding trace elements (Zn, Cu, etc) to the glasses to stimulate cellular proliferation and differentiation.

These results suggest that 13-93B3 bioactive glass scaffolds could serve as effective new substrates for bone repair. Although the borate glass was not shown to promote blood vessel formation, the presence of blood vessels within the scaffold indicates that the boron content of the glass did not have a toxic effect on angiogenesis. Future studies would be needed before borate bioactive glasses are utilized clinically, but these *in vivo* results show that they could be beneficial due to their bone regenerative properties, hydroxyapatite conversion, and ability to be formed into scaffolds that are mechanically strong and customizable to the size and shape of the defect.

Objective G: Multifunctional Bioactive Glass Scaffolds

(G.1) Compositional modification of bioactive glass scaffolds

Compositional modification of the 'parent' or base bioactive glasses (**Table I**) was performed by doping the glass with 'trace' quantities of copper, strontium, zinc, and iron, elements known to promote healthy bone and tissue growth. The compositions of these 'trace element' glasses are given in **Table III**, along with the 'parent' glass composition (13-93B3). Fibrous scaffolds of these 'trace element' glasses, prepared as described earlier, were implanted in subcutaneous pockets in the dorsum of rats. Scaffolds seeded with rat bone marrow-derived stem cells (MSCs) or unseeded were implanted. The implants were evaluated for biocompatibility (local and systemic), and for their ability to promote angiogenesis, the formation of blood vessels.

Table III. Compositions of 'trace element' glasses prepared and evaluated in this work. For comparison, the composition of the 'parent' glass (borate 13-93B3) is also shown.

Composition (wt%)	**B_2O_3**	**CaO**	**K_2O**	**Na_2O**	**MgO**	**P_2O_5**	**CuO**	**SrO**	**ZnO**	**Fe_2O_3**
13-93B3	53	20	12	6	5	4	0	0	0	0
B3 Cu-1	52.95	19.98	11.99	5.99	5.00	4.00	0.10	0	0	0
B3 Cu-3	52.79	19.92	11.95	5.98	4.98	3.98	0.40	0	0	0
CS	51.73	19.52	11.71	5.86	4.88	3.90	0.40	2.00	0	0
CSZ	51.20	19.32	11.59	5.80	4.83	3.86	0.40	2.00	1.00	0
CSZF	50.88	19.20	11.52	5.76	4.80	3.84	0.40	2.00	1.00	0.40

Figure 46a shows pictures of the scaffolds upon removal from the rats after six weeks in subcutaneous tissue. There is a distinct increase in visual blood vessels (red tissue) from the 0 wt% CuO scaffold (left) to the scaffold with 0.4wt% CuO (right). A blinded histological analysis of the area of blood vessels present in the infiltrated tissue showed that the addition of CuO in low concentrations and/or MSCs significantly enhanced ($p<0.05$) the area of blood vessels in the tissue present inside porous fiber scaffolds after six weeks (**Fig. 46b**).

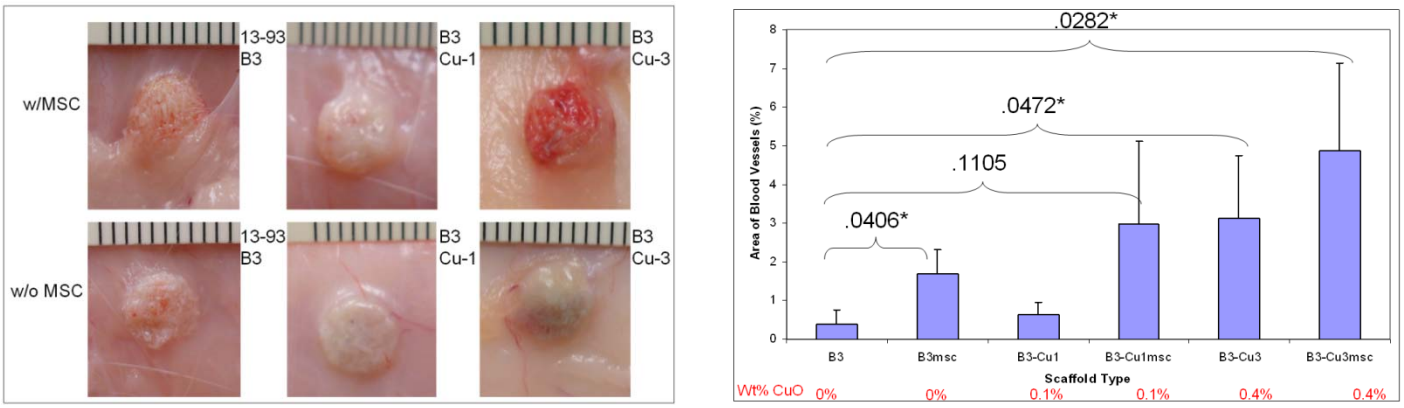

Fig. 46. (a) Photographs of scaffolds upon removal after 6 weeks in subcutaneous tissue in rats; (b) Results of a blinded histological analysis of the area of blood vessels present in the infiltrated tissue of the implants. (Day, Missouri S&T)

During the histological analysis, relatively few inflammatory cells were detected in tissues present inside the porous scaffolds indicating the scaffolds were biocompatible. Macrophages are circled in **Fig. 47(A)**, and it is important to note the cells are spread out in the tissue and not congregating at the fiber (F) surfaces. Blood vessels are denoted by arrows and the vessel wall is a light blue and often contained red blood cells which are light green. In **Fig. 47(B)**, a blood vessel is present within the center of a reacted fiber (arrow), and this is important for a couple reasons. First, it shows the viable tissue can penetrate the reacted borate glass fibers, and second, the blood vessels orient in the longitudinal direction of the fiber which means these bioactive glass fibers may be useful in guiding blood vessels in a desired direction.

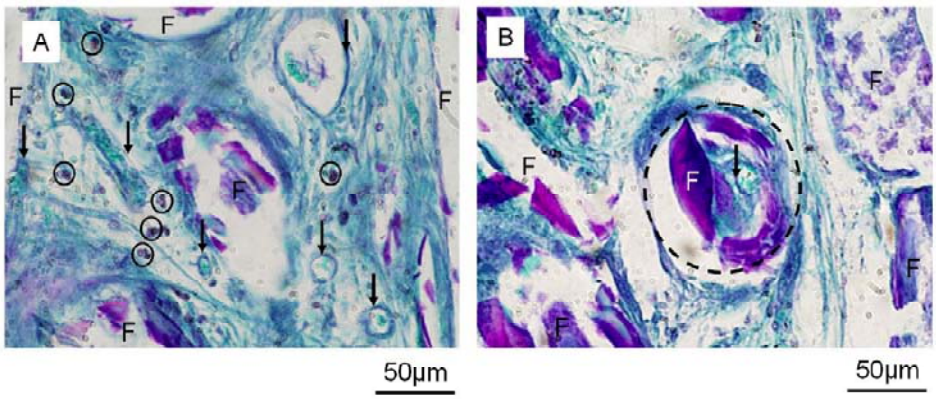

Fig. 47. Optical micrographs of periodic acid-Schiff (PAS) stained sections from a 93B3 scaffold implanted in a subcutaneous tissue for four weeks. Connective tissue is light green, and red blood cells (RBC) are bright green, vessel lining is blue, hydroxyapatite is purple, and macrophages are brown. Figure 35A has stained positive for several blood vessels (arrows) as the blue rings are surrounding bright green RBC. There are several macrophages throughout the tissue, circled; however they are not congregating around the scaffold material (F). Figure 35B has a hollow fiber (F) in the center of the image (dashed circle) with a vessel inside the void (arrow). (Day, Missouri S&T).

The borate glasses studied here improved angiogenesis in the adjacent tissue, and were found biocompatible, with no detectable negative reactions elsewhere in the body (**Table II**). Upon reaction in-vivo, the borate glass fibers became hollow and soft tissues such as blood vessels were detected inside. The reacted hollow fibers could be useful for guiding blood vessels or other tissue such as bone or nerve tissue.

(G.2) Microstructural manipulation of bioactive glass scaffolds for enhanced strength

Bioactive glass scaffolds with either a ‘fibrous’ microstructure (**Fig. 3**) or a ‘trabecular’ microstructure (**Fig. 5**) have been used in the research described so far. Scaffolds with these microstructures have compressive

strength and elastic modulus (**Fig. 4**; **Fig. 8**) comparable to those for trabecular bone, and could be used for the repair of non-loaded bone. To improve the strength of the scaffolds for potential applications in the repair of load-bearing bones, bioactive glass scaffolds with two new microstructures were prepared and evaluated.

Scaffolds with oriented pore architecture prepared by unidirectional freezing of suspensions:
In the first method, scaffolds with an oriented pore architecture were prepared by unidirectional freezing of suspensions of glass particles. Suspensions with an aqueous solvent (water + 60 wt% dioxane) or an organic solvent (camphene) were frozen unidirectionally on a cold substrate. Growth of the ice or camphene crystals down the concentration gradient, followed by freeze drying (sublimation of the ice or camphene), and sintering of the glass particles in the pore walls resulted in the formation of porous constructs with oriented pores (**Fig. 48**). By annealing the frozen constructs prepared from camphene-based suspensions for 0–72 h at 35°C prior to freeze drying and sintering, constructs with different porosities and pore sizes were obtained. **Figure 49** shows X-ray tomography images of a scaffold prepared from camphene-based suspensions, showing the glass phase and the oriented pores.

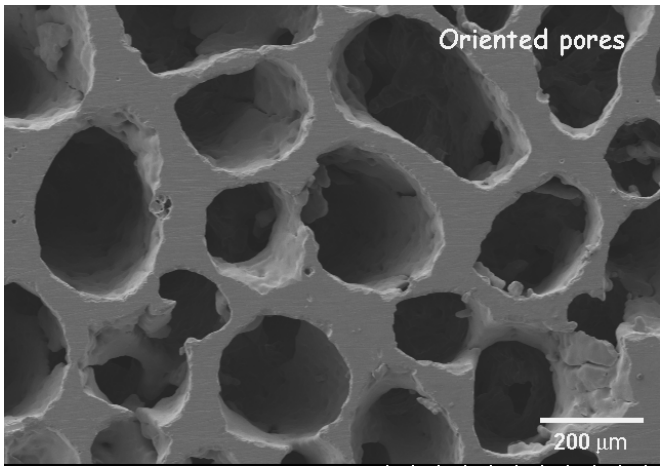

Fig. 48. SEM image of the cross section of 13-93 bioactive glass scaffold prepared by unidirectional freezing of camphene-based suspensions, annealing for 24 h at 35°C, and sintering (1 h at 700°C).

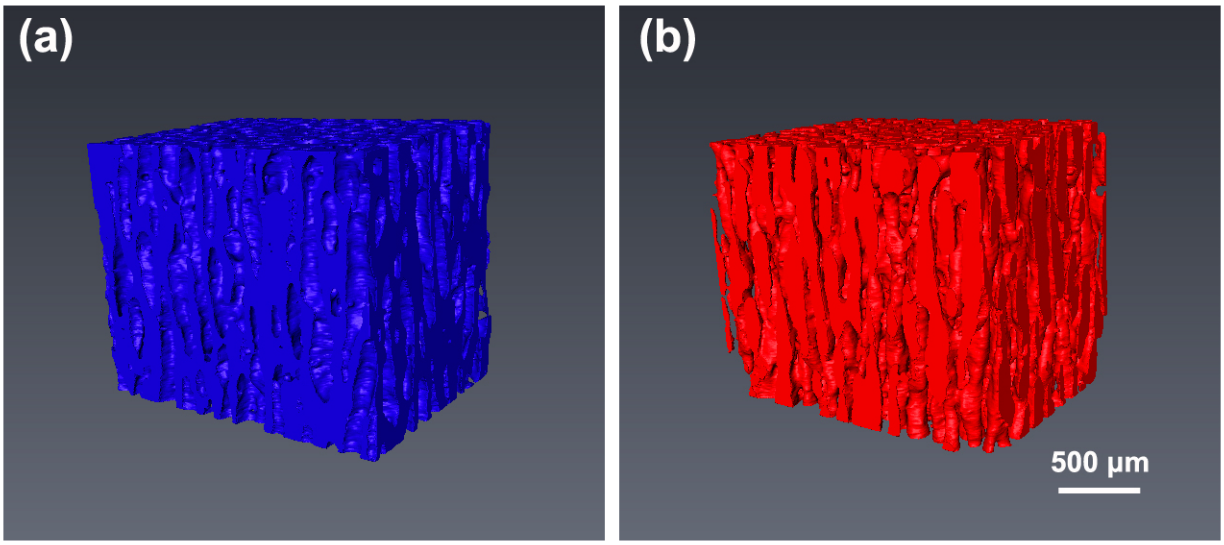

Fig. 49. X-ray tomography images of sintered 13-93 bioactive glass constructs prepared by unidirectional freezing camphene-based suspension at 3°C, annealing for 24 h, and sintering for 1 h at 700°C (glass phase in blue color; pore phase in red color). (Rahaman, Missouri S&T).

The mechanical behavior of cylindrical constructs (8 mm in diameter × 16 mm) in compressive loading was measured according to ASTM-C77 using an Instron testing machine (Model 4881; Instron Corp., Norwood,

MA) at a crosshead speed of 0.05–5.0 mm/min. Eight samples were tested, and the average strength and standard deviation were determined. Scaffolds prepared from aqueous suspensions (porosity = 55–60%; pore width = 90–110 μm) had a compressive strength of 25 ± 3 MPa (deformation rate = 0.5 mm/min) when tested in the direction of orientation, and showed a unique elastic-plastic response, with a large strain for failure (**Fig. 50a**). On the other hand, scaffolds prepared from camphene-based suspensions showed an elastic response (**Fig. 50b**), with compressive strengths (in the orientation direction) ranging from 70 MPa (porosity = 40%; pore width = 40 μm) to 30 MPa (porosity = 50%; pore width = 100 μm).

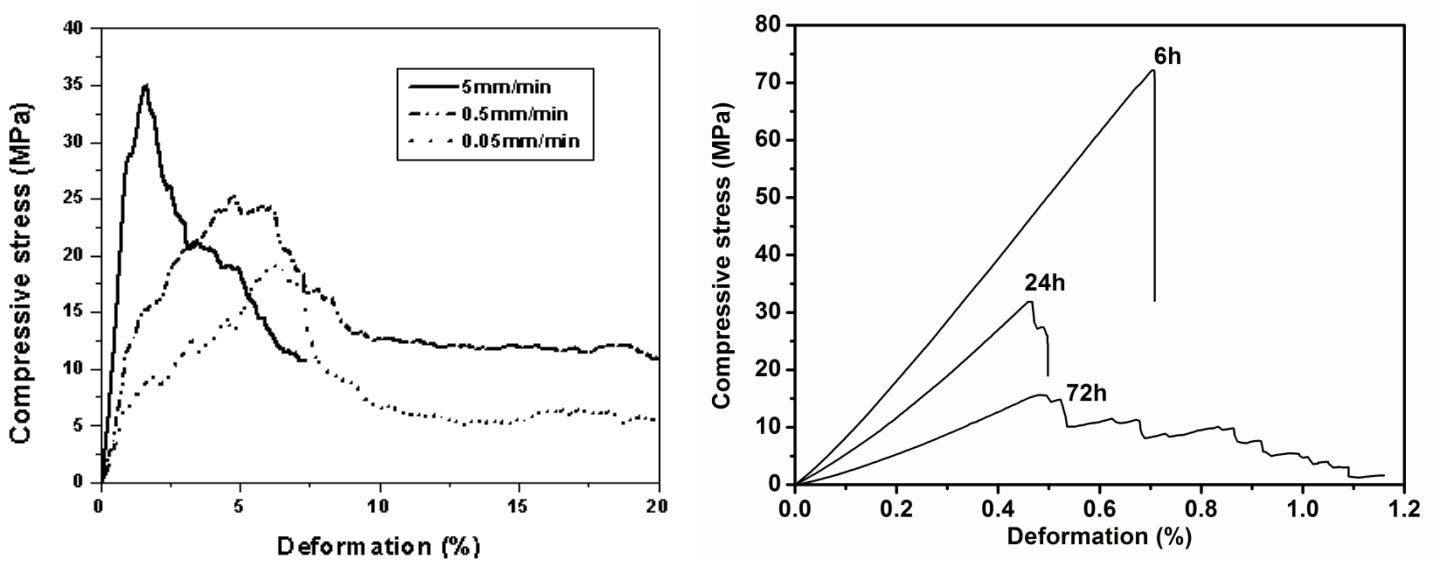

Fig. 50. Compressive stress vs. deformation for 13-93 bioactive glass scaffolds prepared by unidirectional freezing of (a) aqueous suspensions (at the deformation rates shown), and (b) camphene-based suspensions (deformation rate = 0.5 mm/min). The frozen constructs prepared from the camphene-based suspensions were annealed for the times shown, prior to sublimation of the camphene and sintering of the constructs. (Rahaman, Missouri S&T).

As observed from **Fig. 49**, the pores in the "oriented" scaffolds were imperfectly aligned. In the formation of those scaffolds, the suspension was frozen unidirectionally on a cold substrate; the apparatus did not provide the ability to control the cooling rate. A cooling control system (**Fig. 51**) was constructed to provide a better control on the freezing rate of the unidirectional freeze casting method and therefore to improve the alignment of the pores within the scaffolds. A PID controller is employed to control the temperature of the cold finger. The scaffolds showed similar pore diameter and porosity to the scaffolds prepared previously. The mechanical properties of the scaffolds prepared by the controlled cooling equipment were measured. Cylindrical specimens (7 mm in length × 7 mm in height) were machined and tested in compression at a crosshead speed of 0.5 mm/min in an Instron testing machine. For the 6 samples tested, the compressive strength of the scaffolds was 47 ± 5 MPa which is significantly higher than the scaffolds prepared without controlled cooling rate (35 ± 11 MPa). The elastic modulus (10.7 ± 3.3 GPa) was also found to be higher than the uncontrolled one (7.5 ± 2.5 GPa).

Scaffolds with a grid-like microstructure prepared by freeze extrusion fabrication (FEF):
Scaffolds of 13-93 bioactive glass with a designed, grid-like microstructure were also prepared by freeze extrusion fabrication, FEF, a rapid prototyping method. In this method, an aqueous mixture with a paste-like consistency is extruded through an orifice to form filaments, which are frozen *in situ* to avoid slumping or distortion of the formed article. After binder burnout, the constructs were sintered (1 h at 700°C) to densify the glass phase. **Figure 52** shows a fabricated 13-93 bioactive glass scaffold (porosity = 50%; pore width = 500 μm).

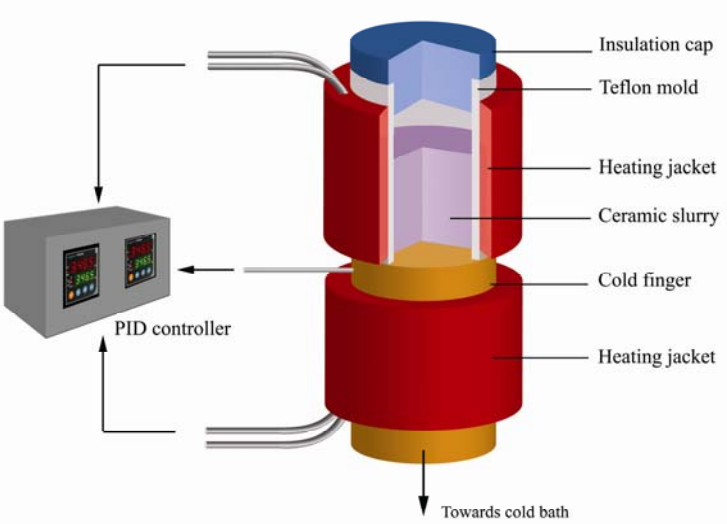

Fig. 51. Schematic of the new cooling control system used for the preparation of “oriented” scaffolds.

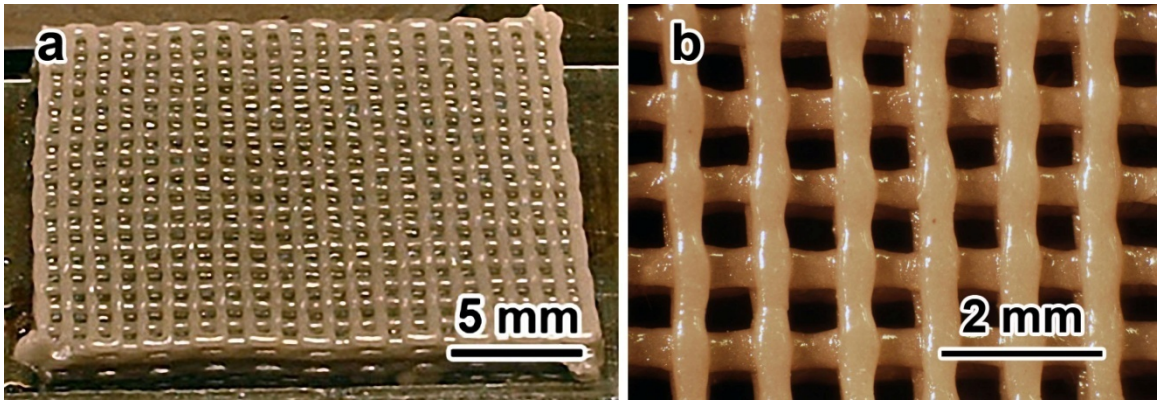

Fig. 52. Optical images showing the structure of the fabricated bioactive glass scaffold (after sintering). (a) entire scaffold; (b): magnified view of the scaffold surface.

SEM images of fractured and polished cross sections of the scaffolds (**Figs. 53a; 53b**) showed that sintering resulted in almost complete densification of the glass phase; the glass struts contained only a few fine, isolated pores. There was good bonding between the adjacent layers of the sintered scaffold. These structural characteristics are desirable for enhancing the overall strength of the sintered scaffold. The pore width in the thickness direction of the scaffold (150−200 μm) was smaller than that in the plane of deposition (~300 μm).

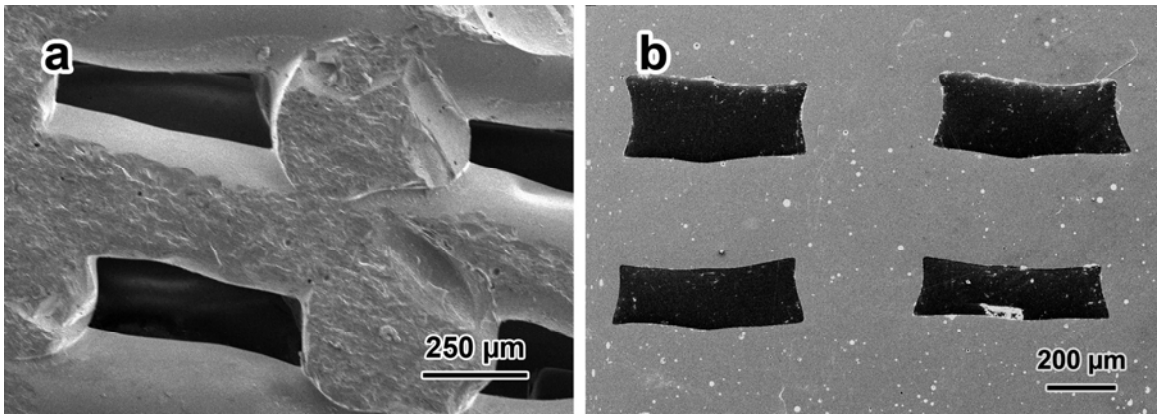

Fig. 53. SEM images of (a) fractured cross section, and (b) polished cross section of the fabricated bioactive glass scaffolds showing (a) good bonding between adjacent layers, and (b) almost full densification of the glass phase. (The section was parallel to the thickness direction of the scaffold.)

The mechanical response of the fabricated scaffolds in compression was measured at a crosshead speed of 0.2 mm/min in an Instron machine (Model 4205; Instron, Norwood, MA). Six cube-shaped samples (5 mm in length) (**Fig. 54a**) were sectioned from the fabricated scaffolds using a diamond-coated blade, and their surface was ground using a diamond-coated wheel. The specimens were tested by applying the load in the thickness direction of the scaffold. The scaffolds showed an elastic response, with a compressive strength of 140 ± 70 MPa and an elastic modulus of 5–6 GPa (**Fig. 54b**), comparable to the values for human cortical bone.

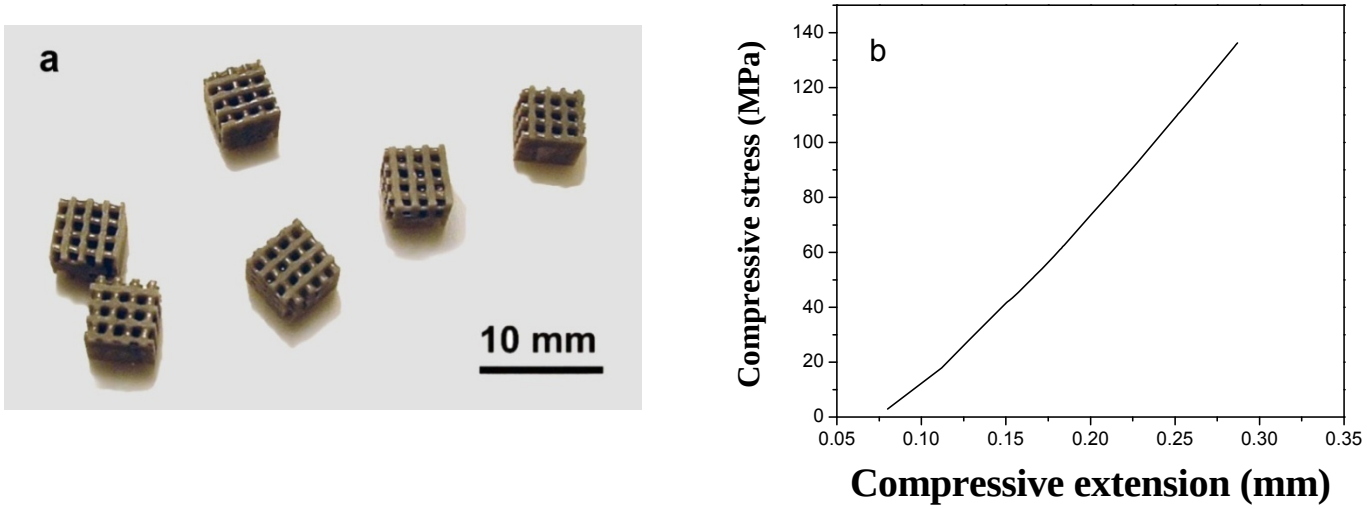

Fig. 54. (a) Cube-shaped samples (5 mm in length) used in mechanical testing; (b) mechanical response (applied stress vs. deformation) of a sample in compression.

Scaffolds with the oriented microstructure, prepared by unidirectional freezing, have been shown to support infiltration of new tissue upon implantation in subcutaneous pockets of rats (Fu et al., 2010), while scaffolds with the grid-like microstructure, prepared by FEF, have been shown to support the proliferation of osteogenic cells. These scaffolds, with their high strength and biocompatibility, could potentially be used in the repair of loaded bone, such as the long bones.

(G.3) Growth factor delivery

A strength of this project is investigating the controlled release of protein growth factors (or antibiotics) from the bioactive glass scaffolds used to replace bone. The addition of a growth factor release function to the porous scaffolds, could provide an approach for the production of multifunctional scaffolds with high mechanical strength coupled with controlled release of growth factors. An inorganic system, hollow hydroxyapatite (HA) microspheres was investigated as a potential delivery device for proteins. These hollow HA microspheres can be bonded to the surface of the bioactive glass scaffold, or incorporated into the pores of the scaffold to provide a device for local delivery of proteins from the scaffolds.

Hollow hydroxyapatite (HA) microspheres (**Fig. 55**) were prepared by reacting solid microspheres of Li_2O–CaO–B_2O_3 glass (106–150 μm) in K_2HPO_4 solution, and evaluated as a controlled delivery device for a model protein, bovine serum albumin (BSA). Reaction of the glass microspheres for 2 days in 0.02 M K_2HPO_4 solution (pH = 9) at 37°C resulted in the formation of biocompatible HA microspheres with a hollow core diameter equal to 0.6 the external diameter, high surface area (~100 m^2/g), and a mesoporous shell wall (pore size ≈ 13 nm).

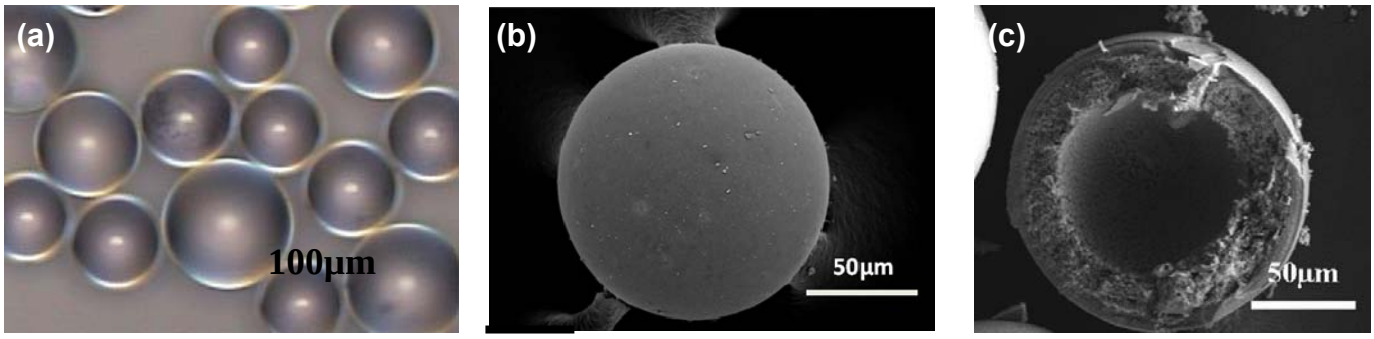

Fig. 55. Optical and SEM images of (a) starting glass (CaLB3-15) microspheres, (b) external surface of hollow HA microsphere formed by conversion of the glass microspheres in K_2HPO_4 solution; (c) cross section of hollow HA microsphere. (Rahaman, Day; Missouri S&T).

After loading with a solution of BSA in phosphate-buffered saline (PBS) (5 mg BSA/ml), the release of BSA from the HA microspheres into a PBS solution were measured using a micro bicinchoninic acid (BCA) protein assay. Release of BSA from the as-prepared HA microspheres was initially rapid (~2.0 µg/ml/h) during the first 10–12 h, then slowed considerably, and almost ceased after 24–48 h (**Fig. 56a**). The total amount of BSA released into the PBS after 14 days was ~22 µg/ml, which was ~44% of the amount of BSA initially loaded into the microspheres. Heating the as-prepared microspheres for 5 h at 600°C resulted in a marked increase in the amount and duration of the BSA released into the PBS. The amount of BSA released was lower than that for the as-prepared microspheres during the first 48–72 h, but continued to increase, and almost ceased after 7–14 days. The total amount of BSA released (after 14 days) was ~35 µg/ml, which was ~30% of the BSA initially loaded into microspheres. For the HA microspheres heated for 5 h at 900°C, release of the BSA from the microspheres into the PBS was limited. The cumulative amount of BSA released after 3–5 h was ~2 µg/ml, and it remained at this value thereafter.

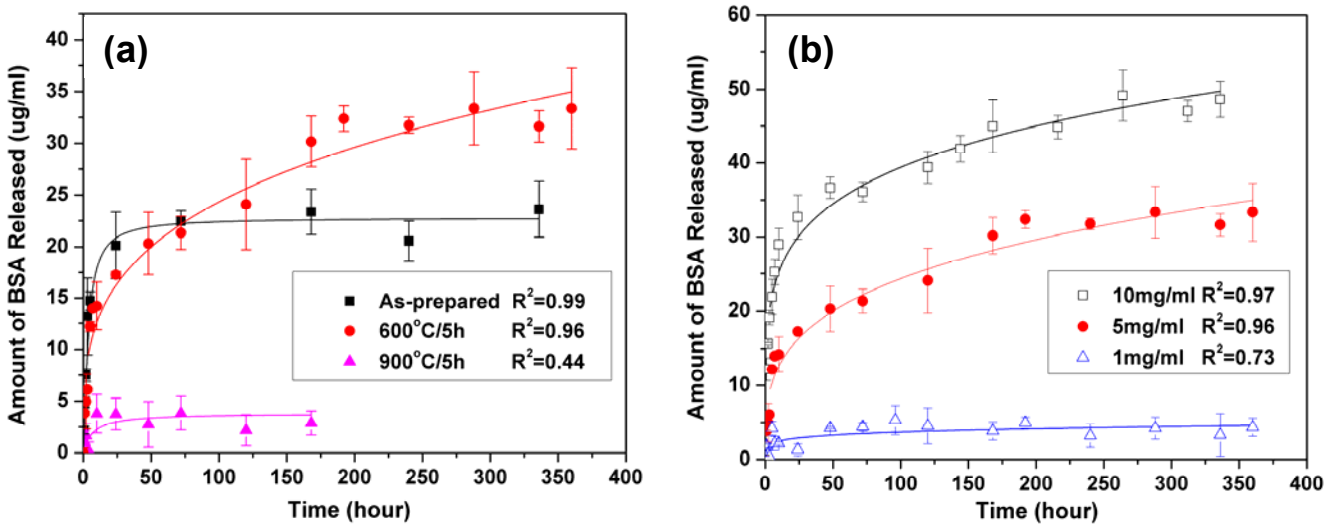

Fig. 56. Amount of BSA released from hollow HA microspheres into PBS, for the as-prepared HA microspheres, and for the HA microsphere heat treated under the conditions shown. (Rahaman, Day; Missouri S&T).

The effect of varying the amount of BSA loaded into the hollow HA microspheres (1–10 mg BSA per ml of PBS) on the release kinetics is shown in **Fig. 56b**. The microspheres used in these experiments were heated for 5 h at 600°C. For a BSA concentration of 1 mg/ml, the total amount of BSA released was limited (~5 µg/ml). Higher BSA loading markedly enhanced the amount of BSA released, as well as the duration of the release. The release kinetics from microspheres loaded with 10 mg/ml BSA followed the same trend as those for microspheres loaded with 5 mg/ml BSA, but the total amount of BSA released was higher (45 µg/ml compared to 35 µg/ml). These hollow HA microspheres are currently being evaluated as a device for controlled delivery os a growth factor, TGF−β.

Biosensor Research and Education (Missouri S&T): A Simple Oxygen Imaging Method for Continuous Monitoring of Bioactive Glass Conversion Process

Investigators: Henthorn and Kim

Need for oxygen imaging

Tissue regrowth and wound healing requires maintenance of optimal levels of metabolites (e.g. oxygen, ions, pH and glucose, etc.). Current biosensor work at Missouri University of Science and Technology's Center for Bone and Tissue Repair and Regeneration focused on developing optical biosensors to monitor oxygen. Molecular oxygen is one of the most vital species involved in biochemical cycles, and oxygen determination is critical in many applications. Therefore, oxygen monitoring is important in the fundamental study of conversion mechanism from bioactive glass, soft tissue wound healing, and general health of the growing cells on artificial tissue scaffolds. The goal of this study was to design, fabricate, calibrate, and test an optical biosensor to map the oxygen distribution around bioactive glass scaffold during conversion to hydroxyapatite (HA). It is anticipated that feedback from these sensors will aid in refining bioactive glass formulation and designing glass scaffold structure, allowing researchers to better understand how desired levels of analyte molecules are maintained in the complex process of tissue ingrowth.

A simple oxygen imaging method based on color camera and oxygen sensor film

Partially supported by this grant, we have demonstrated a simple oxygen imaging method utilizing commercial oxygen sensor patches and a color CCD camera. These results are available publicly (see REPORTABLE OUTCOMES). This final report summarizes our subsequent work done focusing on monitoring bioactive conversion process in simulated physiological solution environment. As shown in **Fig. 57**, we developed a simple oxygen imaging platform with lab-made phosphorescent oxygen sensor films. Test cell (petri dish) with its bottom coated with PtTFPP/PDMS membrane from within, was sealed, with an inlet and outlet drilled into its cap. The test cell was completely filled (without any air gap) with phosphate buffer solution. A bioactive glass scaffold disc was placed at the center of the petri dish. Oxygen distribution was monitored radially away from the glass surface over time by taking images from the petri dish bottom.

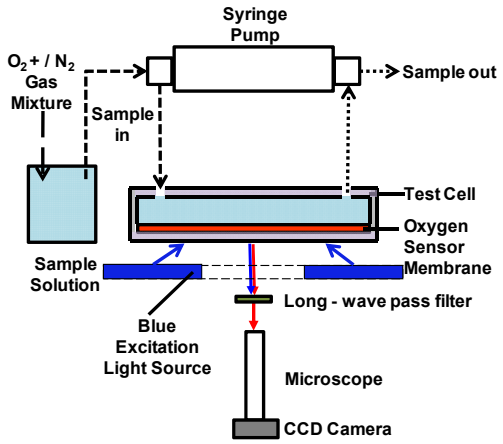

Fig. 57. A simple oxygen imaging setup with an oxygen sensor film on the bottom of test cell and a color CCD camera to map oxygen distribution within the bioactive glass scaffold and its surrounding phosphate buffer solution during the conversion process. Data was collected both with and without the long-wave pass filter.

A camera using a charge-coupled device (CCD) was used in conjunction with processing software to colorimetrically quantify oxygen levels. The color CCD camera allows simultaneous acquisition of many types of chemical information by combining the merits of digital imaging with the attributes of spectroscopic measurement. CCD cameras are potentially valuable tools in chemical quantification purposes such as the simultaneous analysis of multiple-targets. Microscopic images were collected using a CCD camera and stored as a set of red/green/blue (RGB) images. Phosphorescence excitation is limited to the blue channel and these values are discarded. Phosphorescence emission, on the other hand, is mostly limited to the red channel and information of the oxygen environment throughout the scaffolds and its vicinity is obtained from these values. The oxygen related emission range of the PtTFPP complex is almost identical with the response range of the

red (R) subpixels of the CCD chip used for measurement. Therefore, only the red color spectral sensitivity in the figure remained after the red color extraction process. Alternatively, a long-wave pass filter (cut-on wavelength 500 nm) in front of the CCD camera was used to eliminate the strong blue excitation light to enhance oxygen sensitivity.

Current work on oxygen quantification employs a sensitive ionophore Pt(II) meso-tetrakis (pentafluorophenyl) porphine complex (PtTFPP) immobilized in poly (dimethylsiloxane) (PDMS) matrix, and cast to form a film. The principal detection mechanism was the luminescence quenching of PtTFPP. As levels of dissolved oxygen increase, luminescence of the complex decrease, allowing for the measurement of two-dimensional oxygen gradients which develop in the sensor film. Colorimetric analysis of this film allows us to generate a color-coded picture of the oxygen gradient that exists in and around the degrading bioactive glass scaffold. PtTFPP/PDMS combination was chosen since this sensor features a strong Stern – Volmer (SV) response that is spatially homogenous on length scales ranging from few micrometers to several millimeters. PDMS was finalized for immobilizing the complex due to the its excellent oxygen permeability, optical transparency, and rigidity. Dye aggregation has been known to cause high variability in oxygen response, nonlinear Stern - Volmer plots, and uneven background emission that limits integration. When compared to other dyes, the PtTFPP is relatively nonpolar and thus soluble in PDMS polymer matrix without any dye aggregation or phase separation.

19.6 mg Pt(II) meso-tetrakis (pentafluorophenyl) porphine complex (PtTFPP, Frontier Scientific Inc., Logan, Utah, USA) was stirred in 1.8 ml of toluene for 10 min and thoroughly mixed with 6.6 ml solution of 10 parts polydimethylsiloxane prepolymer (PDMS, Sylgard 184, Dow - Corning, MI, USA) to 1 part curing agent for another 30 min. A 0.5 ml portion of this mixture was spin-coated in a 54 mm diameter polystyrene petri dish to obtain a 130 μm thick film. Spin-coating was chosen as the fabrication strategy since it can be rapidly adapted to a variety of sensor geometries. An aliphatic hydrocarbon solvent like toluene helps dilute the prepolymer (0.93 g/cm^3 density) and adjust film thickness. Toluene was allowed to evaporate overnight while the polymer cured. Atmospheric moisture hydrolyzes the methoxy group to form silanol groups, which condense with silanol or methoxy groups to liberate water or methyl alcohol and form new siloxane bonds. Soft, clear rubbery films result. The curing time is temperature dependent; at room temperature, the membrane must cure for about 16 to 24 hours, at 70^{o}C it must cure for 4 h, and at 90^{o}C it must cure for 2 h. The optimum PtTFPP concentration in the final membrane ranges from 0.001 to 2 mM, consequently the final PtTFPP sensor film had a dye concentration of 2 mM.

Oxygen sensor film characterization

First, excitation/emission spectra of the PtTFPP/PDMS sensor film were measured by a conventional reflection probe spectrometer (USB2000-FLG, Ocean Optics, USA) with a 45 μW blue LED (LS450, output wavelength 380 nm, Ocean Optics, USA) as an excitation source. Phosphorescence data obtained for the sensor films represents the average over a small patch (equivalent to an active area of a reflection probe 400 μm diameter) of the sensor membrane. The phosphorescence emission peak intensity of 645 nm dropped as oxygen concentration increased, as shown in **Fig. 58**.

Response time was also measured using the same spectrometer. The response/detection/stabilization time of optical sensors (based on luminescence quenching) is defined as the time required to reach 95% of the final response. Thus, oxygen sensor film response times were recorded for a rise in oxygen levels from 0 to 21% and a fall back to 0%. Variations in response time with respect to membrane thickness were also studied. The film has a response time (to reach 95% of signal change) of ~ 3 min when the oxygen level was increasing (from 0 to 21%), and ~ 3.5 min as for decreasing (21 to 0%) oxygen concentrations. **Fig. 59** demonstrates the variation in response time with membrane thickness. The long response time is likely due to the high solubility of oxygen in siloxanes, which can cause undesirably strong quenching of long-decay phosphorescent dyes in the polymer phase at physiological oxygen concentrations. A film thickness of 130 um was determined to be optimal because it adhered best to the substrate and was mechanically strong.

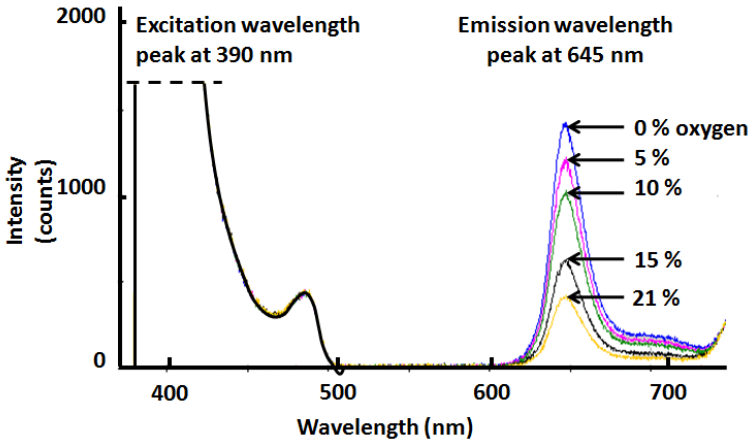

Fig. 58. Luminescence spectra of PtTFPP/PDMS complex, with decreasing emission intensity at 0, 5, 10, 15, 21% oxygen saturation percentage in phosphate buffer solutions.

Oxygen sensitivity was measured with a color camera (DS-5M-L1, 5-megapixel, Bayer masked, Nikon) employing a CCD (ICX282AQ, Sony). A long-wave pass filter (10LWF-500-B, cut-on wavelength 500nm, Newport) was used at the receiving end to eliminate the intense blue wavelength range from the sensor images. A reflected light illumination method was employed, wherein the specimen was lit and the light reflected from it was observed, with the illumination and imaging equipment stationed on the same side/below the test cell. A ring array of excitation LEDs (395 nm wavelength, 0.73 mW/cm^2 flux, 30 mm working distance, with inbuilt diffuser, Edmund Optics, USA) ensured the sample membrane was illuminated uniformly all round, eliminating occurrence of the scaffold's shadow in the image. The camera exposure time was 60 seconds. The absolute intensity of the images in **Fig. 60(a)** decreases as the oxygen percentage in the solution increases due to oxygen quenching. As shown in **Fig. 60(b)**, the CCD camera method performed well over the range of oxygen concentrations of interest. A traditional plot of normalized intensity (I_0/I vs. oxygen concentration; I_0= intensity at 0% O_2 and I = intensity at certain 0% O_2) is shown in **Fig. 60(c)** to compare with the linear Stern-Volmer equation. Error bars indicate the standard deviation of the mean of five independent measurements. All images were analyzed using NIH ImageJ software (http:// rsbweb.nih.gov/ij/).

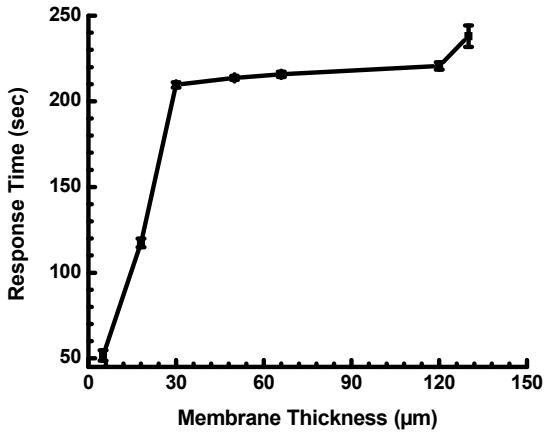

Fig 59. PtTFPP/PDMS sensor film response time with changing film thickness measured with a spectrometer at its peak emission wavelength (645 nm).

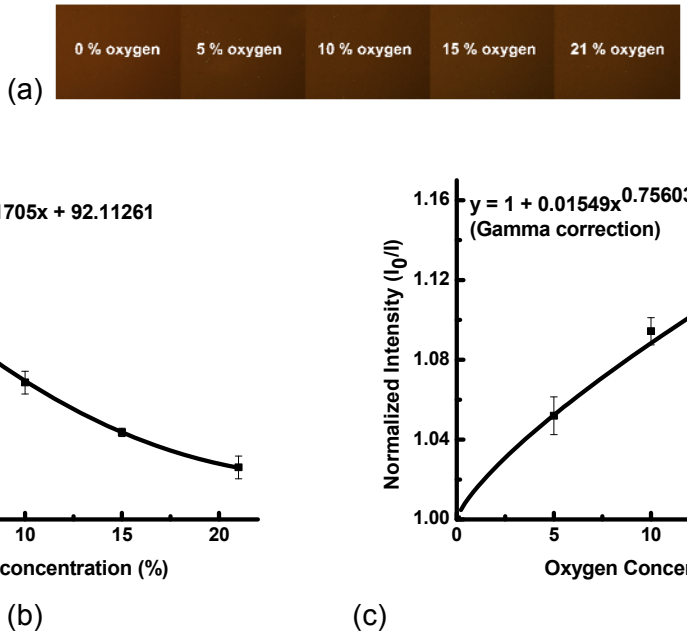

Fig. 60. Oxygen sensitivity of PtTFPP/PDMS sensor film measured with a CCD camera: (a) sensor film images and (b) variation of mean absolute red (R) channel intensity with changing oxygen level, (c) Stern-Volmer calibration plot (I_0/I vs. oxygen concentration; I_0= intensity at 0% O_2 and I = intensity at certain 0% O_2) after camera gamma-correction induction

Monitoring of bioactive glass conversion

Figure 61 (a) shows the sensor film images taken from the bottom of petri dish in which a portion of a 1393B3 glass scaffold disc (diameter about 5 mm) is seen through the translucent sensor film. The glass appears denser with precipitated hydroxyapatite (HA) in the second picture (after 72 hr). After 58 hours, solid deposition was observed on the sensor film around the glass. This whitish precipitate affected intensity measurements in the late hours of the monitoring. A white, porous layer was used to minimize this artifact while maintaining transport of oxygen to the sensor film. As in **Fig. 61(b)**, filter paper (MAGNA, Nylon, Supported, Plain, 0.45 Micron, 90 mm, Osmonics Inc., MN, USA) was lined over the sensor film and the glass placed on top of it. Reaction byproducts settled over the filter paper and thus interfered less with intensity measurements.

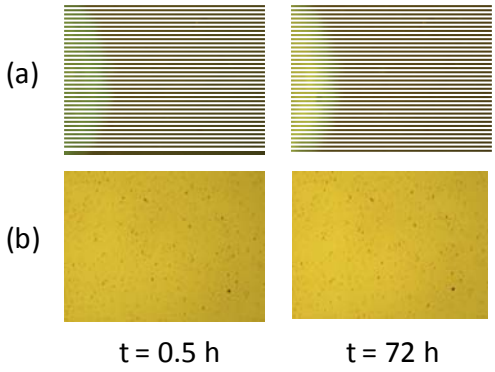

Fig. 61. Sensor film images from the bottom of petri dish (a) without and (b) with white filter paper to minimize the optical artifact caused by solid precipitation during bioactive glass conversion process in 10 mM phosphate buffer solution.

Figure 62(a) depicts the distribution of oxygen-responsive sensor emission radially away from a 1393 glass scaffold disc. The first millimeter away from the graphs' origin depicts sensor film area under the scaffold, enabling oxygen mapping within the scaffold. Beyond the location of 1 mm (i.e. the interface of glass and solution), emission intensity is plotted for another 4 mm away from the glass edge toward bulk solution. At time

zero, oxygen was purged from the sensing setup to measure baseline intensity as a function of radial distance. As shown in **Fig. 62**, all luminescence measurements show increased intensity near the scaffold (closer to the center of microscope image). This is attributed to the radial profile of excitation illumination intensity.

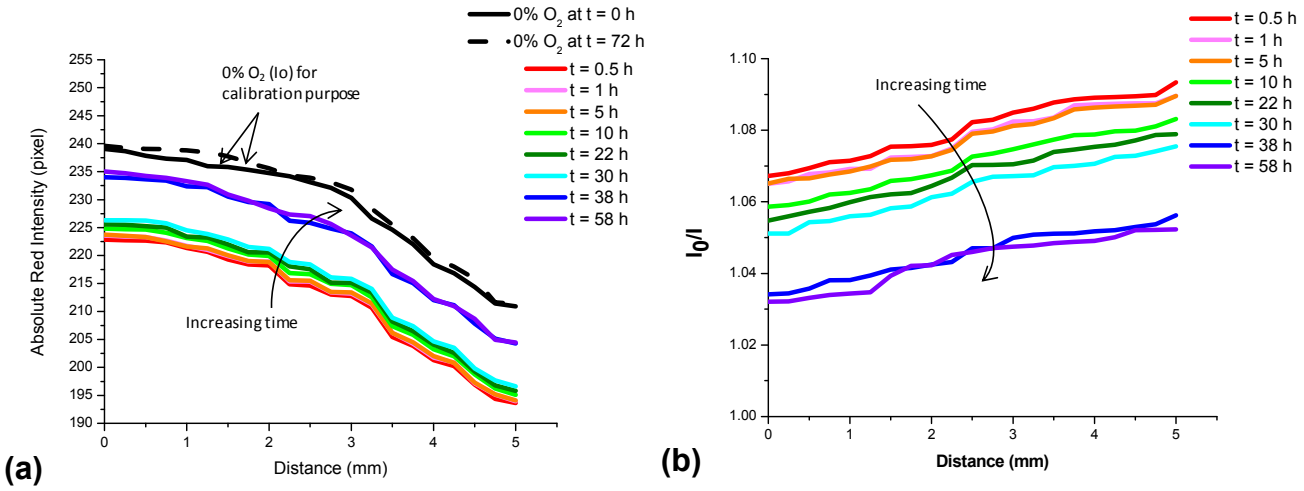

Fig. 62. (a) Typical absolute red (R) channel intensity around a bioactive glass scaffold (1393) over time in 10 mM phosphate buffer solution, (b) SV plot (I_0/I=1.095 being 21% oxygen saturation equivalent with air-saturated solution and I_0/I=1.000 being 0% oxygen saturation, respectively).

To reduce the effect of uneven illumination intensity, the intensity measured at a given radial distance was normalized against the baseline intensity (I_0) at that same spot. These values were then plotted as I_0/I versus radial distance, in accordance with the expected Stern-Volmer dependence. Despite this normalization, it is apparent that oxygen concentration in the sample cell decreases with time, and a significant oxygen concentration gradient develops radially. The rise in absolute intensity with time can be attributed either to oxygen consumption in the conversion reaction of the scaffold, or to a lowering of oxygen solubility in the presence of a number of competing solutes. A steep oxygen gradient develops, possibly due to diffusion of ions from the scaffold into the surrounding solution (counterdiffusion) as the reaction progresses. During conversion of glass to HA, there is a great efflux of Na^+, K^+, Ca^{2+}, $(BO_3)^{3-}$ ions from the glass into the surrounding solution. This potentially reduces oxygen solubility of the solution, which may be responsible for oxygen appearing to have been depleted with time around the scaffold. This result warrants further investigation to elucidate its cause and to explain possible conversion mechanisms.

Color CCD imaging is an inexpensive alternative to fluorescence time-resolved imaging. Red pixel intensity analysis with a color CCD for oxygen responsive emission effectively extracts color/chemical information. The acquired image can be processed by conventional image processing software to extract the red color component from the original RGB color image and to directly relate it to oxygen content in the sample. Following calibration, interferant, and stability measurements, the oxygen distribution around reacting bioactive glass scaffolds was observed over a short reaction time of 72 hours. Data shows that oxygen is depleted in the area closest to the scaffold and that an oxygen gradient develops radially away from the scaffold. This result suggests that reaction conditions yield oxygen-depleted conditions within the scaffold during conversion. Future work will focus on the implantation of sensor membranes at the wound site to study *in vivo* regeneration. Levels of oxygen at the wound sites will be monitored and correlated with optical images of tissue regrowth.

KEY RESEARCH ACCOMPLISHMENTS

- Prepared and evaluated scaffolds of three candidate bioactive glasses with silicate (13-93), borosilicate (13-93B1), and borate (13-93B3) composition;
- Showed that borate bioactive glass (13-93B3) could serve as an effective new scaffold material for bone and soft tissue repair;
- Tests of mechanical properties showed that scaffolds of 13-93, 13-93B1, or 13-93B3 glass could be used for the repair of loaded bone, as well as non-loaded bone;
- Implantation in rat calvaria defects showed the potential of borate 13-93B3 glass to enhance new bone formation (when compared to silicate 13-93 glass with the same microstructure);
- Incorporation of trace quantities of elements (such as 0.4 wt% copper) into borate 13-93B3 glass, and/or seeding the scaffolds with bone marrow derived mesenchymal stem cells promoted angiogenesis in scaffolds implanted subcutaneously or in the calvaria of rats;
- Demonstrated a simple quantitative oxygen imaging method with color CCD camera to monitor the oxygen environment during the bioactive glass conversion process in saline solution.
- Explored feasibility of a simple transcutaneous wound healing monitoring devices utilizing the developed sensor films and color camera based photometric methods.

REPORTABLE OUTCOMES

Patents
Delbert E. Day, Steven B. Jung, Scaffold For Bone and Tissue Repair In Mammals, United States Patent Publication US 2010/0179667 A1, 7/15/2010.

U.S. Patent Application Serial No. 12/683,211 ‘Controlling vessel growth and directionality in mammals and implantable material’. Filed 1/6/2010.

U.S. Patent Application Serial No. 12/683,244 ‘Wound care.’ Filed 1/6/2010.

U.S. Patent Application Serial No. 12/683,280 ‘Compositions with trace copper for tissue regeneration in mammals.’ Filed 1/6/2010.

International Patent Application No. PCT/US2010/48778 ‘Controlling calcium compound formation in biocompatible materials for tissue regeneration and repair in mammals.’ Filed 9/14/2010.

Manuscripts

Fu Q, Rahaman MN, Bal BS, Brown RF (2010). Preparation and in vitro evaluation of bioactive glass (13-93) scaffolds with oriented microstructures for repair and regeneration of load-bearing bones. J Biomed Mater Res Part A 93A;1380–1390.

Fu Q, Rahaman MN, Fu H, Liu X (2010). Silicate, borosilicate, and borate bioactive glass scaffolds with controllable degradation rates for bone tissue engineering applications, I: Preparation and in vitro degradation. J Biomed Mater Res Part A 95A;164–171.

Fu Q. Rahaman MN, Bal BS, Bonewald LF, Kuroki K, Bown RF (2010). Silicate, borosilicate, and borate bioactive glass scaffolds with controllable degradation rates for bone tissue engineering applications, II: In vitro and in vivo biological evaluation. J Biomed Mater Res Part A 95A;172–179.

Fu Q, Rahaman MN, Bal BS, Kuroki K, Brown RF (2010). In vivo evaluation of 13-93 bioactive glass scaffolds with trabecular and oriented microstructures in a subcutaneous rat implantation model. J Biomed Mater Res Part A 95A;235–244.

Huang TS, Rahaman MN, Doiphode ND, Leu MC, Bal BS, Day DE, Liu X (2011). Freeze extrusion fabrication of 13-93 bioactive glass scaffolds for repair and regeneration of load-bearing bones. Proceedings of MS&T 10, Houston, TX, October 17-21. In press.

Jung SB, Day DE, Brown RF (2010). Comparison of self-bonded, three dimensional bioactive glass fiber scaffolds after in-vivo implantation. Advances in Bioceramics and Biotechnologies, Edited by R. Narayan and J. McKittrick. Ceramic Trans 218;115-132.

Liu X, Rahaman MN, Fu Q (2011). Oriented bioactive glass (13-93) scaffolds with controllable pore size by unidirectional freezing of camphene-based suspensions: microstructure and mechanical response. Acta Biomater 7:406-16.

Park J, Kim C-S. A simple quantitative oxygen imaging method with white LED and color CCD, Sensor Letters (2010); in press.

Park J, Hong W, Kim C-S. Color intensity method for hydrogel optical sensor array, IEEE Sensors Journal, (2010); in press.

Rahaman MN, Fu Q, Bal BS, Day DE, Fu H (2010). Bioactive glass for bone and joint repair. Advances in Bioceramics and Biotechnologies, Edited by R. Narayan and J. McKittrick. Ceramic Trans 218.

Presentations

Day DE, Jung S. Evaluation of three-dimensional scaffolds made from 13-93 and 45S5 bioactive glass fibers after in-vivo implantation in rats. Invited Presentation, 8th Pacific Rim Conference on Ceramics and Glass Technology, Vancouver, BC, Canada, May 31-June 5, 2009.

Fu Q, Rahaman MN, Tomsia AP. Novel Biodegradable and Bioactive 13-93 Glass Scaffolds for Bone Tissue Engineering American Ceramic Society, Glass and Optical Materials Division, Corning, NY; May 16–19, 2010.

Huang TS, Rahaman MN, Doiphode ND, Leu MC, Bal BS, Day DE, Liu X (2011). Freeze extrusion fabrication of 13-93 bioactive glass scaffolds for repair and regeneration of load-bearing bones. *MS&T 10*, Houston, TX, October 17-21.

Jung SB, Day DE. Comparison of self-bonded three dimensional bioactive glass fiber scaffolds after in-vivo implantation in rats. International Materials Institute US-China Winter School, Hang Zhou, China, January 2010

Liu X, Rahaman MN, Fu Q. Unidirectional Bioactive Glass (13-93) Scaffolds with Controllable Pore Size for Repair of Load-Bearing Bones. Society for Biomaterials, 2010 Annual Meeting & Exposition, Seattle, WA, April 21–24, 2010.

Modglin V, Brown RF, Fu Q, Rahaman MN. Growth and function of MLO-A5 cells on 13-93 glass trabecular scaffolds. Poster presentation, Society for Biomaterials Annual Meeting, San Antonio, TX, April, 2009.

Modglin V, Brown RF, Jung S, Day DE. Performance of 13-93 glass fiber scaffolds with osteogenic cells. Poster presentation, Society for Biomaterials Annual Meeting, San Antonio, TX, April, 2009.

Rahaman MN. Bioactive glass for bone and joint repair. Invited Presentation, 8th Pacific Rim Conference on Ceramics and Glass Technology, Vancouver, BC, Canada, May 31-June 5, 2009.

Degrees (awarded) which were Supported by this Award

Modglin V. Master of Science in Applied and Environmental Biology. Thesis: '*In Vitro* Evaluation of Bioactive Glass Scaffolds and Modified Bioactive Glasses with an Osteogenic Cell Line'. Missouri University of Science and Technology, July, 2009.

Fu Q. Doctor of Philosophy in Ceramic Engineering. Thesis: 'Freeze Casting of Bioactive Glass and Ceramic Scaffolds for Bone Tissue Engineering'. Missouri University of Science and Technology, August, 2009.

Jung SB. Doctor of Philosophy in Materials Science and Engineering. Thesis: 'Borate Based Bioactive Glass Scaffolds for Hard and Soft Tissue Engineering', Missouri University of Science and Technology, August, 2010.

Degrees (in progress) which were Supported by this Award

Liu X (Candidate for Doctor of Philosophy in Ceramic Engineering). Title of project: 'Bioactive glass scaffolds for the Repair and Regeneration of Loaded Bone'.

Bhagwat P. (Candidate for Master of Science in Chemical and Biological Engineering). Title of project: Integration of Biosensors into Wound Sites.

CONCLUSION

Porous three-dimensional bioactive glass scaffolds have considerable promise for the repair and regeneration of hard and soft tissues. When compared to the widely studied silicate bioactive glasses, borate bioactive glasses could serve as effective new scaffold materials for bone repair. Scaffolds of silicate or borate bioactive glass could be used for the repair of loaded bone, as well as non-loaded bone. When doped with trace quantities of elements such as copper and/or seeded with mesenchymal stem cells, borate bioactive glass scaffolds can enhance new bone growth and angiogenesis.

REFERENCES

Brown RF, Day DE, Day TE, Jung S, Rahaman MN, Fu Q (2008). Growth and differentiation of osteoblastic cells on 13-93 bioactive glass fibers and scaffolds. *Acta Biomater* 4:387-96.

Davis DH, Giannoulis CS, Johnson RW, Desai TA (2002). Immobilization of RGD to silicon surfaces for enhanced cell adhesion and proliferation. Biomaterials 23:4019-27.

Fu Q, Rahaman MN, Brown RF, Bal BS, Day DE (2008). Mechanical and in vitro evaluation of 13-93 bioactive glass scaffolds prepared using a polymer foam replication technique. Acta Biomater 4:1854–1864.

Fu Q, Rahaman MN, Bal BS, Kuroki K, Brown RF (2010). In vivo evaluation of 13-93 bioactive glass scaffolds with trabecular and oriented microstructures in a subcutaneous rat implantation model. J Biomed Mater Res Part A 95A:235-244.

Fu Q, Rahaman MN, Fu H, Liu X (2010). Silicate, borosilicate, and borate bioactive glass scaffolds with controllable degradation rate for bone tissue engineering applications. I. Preparation and in vitro degradation. J Biomed Mater Res A 95A:164-171.

Fu Q, Rahaman MN, Bal BS, Bonewald LF, Kuroki K, Brown RF (2010). Silicate, borosilicate, and borate bioactive glass scaffolds with controllable degradation rate for bone tissue engineering applications. II. In vitro and in vivo biological evaluation. J Biomed Mater Res A 95A:172-179.

Giannoudis PV, Dinopoulos H, Tsiridis E (2005). Bone substitutes: an update. Injury. Nov;36 Suppl 3:S20-7.

Gorustovich AA, López JM, Guglielmotti MB, Cabrini RL (2006). Biological performance of boron-modified bioactive glass particles implanted in rat tibia bone marrow. Biomed Mater 2006;1(3):100-5.

Hench LL, Splinter RJ, Allen WC, Greenlee TK (1971). Bonding mechanisms at the interface of ceramic prosthetic materials. J Biomed Mater Res 5:117-141.

Hench LL (2006). The story of Bioglass. J Mater Sci Mater Med 17(11):967-78.

Hu YC, Zhong JP (2009). Osteostimulation of bioglass. Chin Med J (Engl). 5;122(19):2386-9.

Huang W, Day DE, Kittiratanapiboon K, Rahaman MN (2006). Kinetics and mechanisms of the conversion of silicate (45S5), borate, and borosilicate glasses to hydroxyapatite in dilute phosphate solutions. J Mater Sci Mater Med 17:583–596.

Kato Y, Boskey A, Spevak L, Dallas M, Hori M, Bonewald LF (2001). Establishment of an osteoid preosteocyte-like cell MLO-A5 that spontaneously mineralizes in culture. J Bone Min Res 16:1622–33.

Kokubo T, Kushitani H, Sakka S, Kitsugi T, Yamamuro T (1990). Solutions able to reproduce in vivo surface-structure changes in bioactive glass-ceramic A-W. J Biomed Mater Res 24:721–734.

Liu X, Pan H, Fu H, Fu Q, Rahaman MN, Huang W (2010). Conversion of borate-based glass scaffold to hydroxyapatite in a dilute phosphate solution. Biomed Mater. 5(1):15005.

Rucker M, Laschke MW, Junker D, Carvalho C, Schramm A, Mulhaupt R, Gellrich N, Menger MD (2006). Angiogenic and inflammatory response to biodegradable scaffolds in dorsal skinfold chambers of mice. Biomaterials 27:5027–38.

Sabokar A, Millett PJ, Myer B, Rushton N (1994). A rapid, quantitative assay for measurine alkaline phosphatase in osteoblastic cells *in vitro*. Bone Miner 27:57–67.

Schmitz JP, Hollinger JO (1986). The critical size defect as an experimental model for craniomandibulofacial nonunions. Clin Orthop Relat Res 205:299-308.

Wolfe SA (1982). Autogenous bone grafts versus alloplastic material in maxillofacial surgery. Clin Plast Surg 9(4):539-40.

Yao A, Wang D, Huang W, Fu Q, Rahaman MN, Day DE (2006). In vitro bioactive characteristics of borate-based glasses with controllable degradation behavior. J Am Ceram Soc 90:303-306.